Design and optimisation of damped cable system characteristics to suit application

European Commission
Energy, Environment
and Sustainable
Development

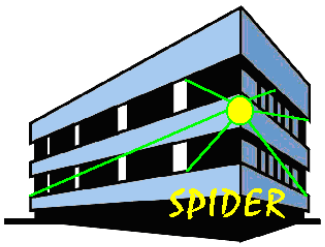

EVG1-CT-1999-00013 SPIDER

WORKPACKAGE 1 – TASK 1.1

Deliverable D1

Design and optimisation of damped cable system characteristics

Stefano SORACE, Ivana AGNOLIN, Sebastiano SURACI
(Università di Udine)

Gloria TERENZI
(Università di Firenze)

EVG1-CT-1999-00013 SPIDER/1.1/ UDINE/SSO/01/VF-C

December 2000

Premise

The activities carried out by Udine University within Work-package nr. 1 ("Identification of structural typologies and of the requested damper/cable system characteristics"), for which it has had the role of task leader, consisted of the following main aspects:

- elaboration of a finite element calculus code to model seismic response of frame and dual structures, incorporating damped cable (DC) protective system;
- development of a wide numerical enquiry by means of this code, with the view of parametrically analysing the effects of the main mechanical quantities and design assumptions on performance of DC technology, as well as of identifying the structural typologies for which it can provide significant advantages (already assessing possible limitations and problems for practical implementation of the protective strategy);
- location of preferable ranges of variation of the most critical mechanical parameters, by which to provide useful information for the construction of prototypes to be tested within Work-package nr. 2;
- development of a preliminary numerical analysis on the mock-up building to be tested within Work-package nr. 7, so as to pre-evaluate dimensions and performance features of the system to be applied for that experimental campaign.

The outcome of this activities is summed up in sections 1 through 4, enclosed to this report.

The aspects listed above entirely cover the previously planned work, compared to which a fundamental additional contribution is represented by the elaboration of the new finite element code cited at the first point.

The choice of defining a new code since the beginning of this research was due to the inherent limitations recognized in numerical models already available, a preliminary use of which had been suggested in the originally planned work program.

In doing so, an effective computational platform over which to develop a simplified tool for the design of structures to be equipped with DC technology — that represents an objective to be pursued within Work-package nr. 5 — has yet been established.

Further implementation of this code, essentially consisting of its extension to 3-D analysis as well as of the addition of new library elements, will be the main aims of the work to be performed during the next six months. Other objectives are constituted by a co-operation with the other Partners to best define the set-up for tests on DC prototypes (Task 2.4), and a refinement of mock-up numerical model, to be accomplished on the basis of a more detailed mechanical characterization of the test-structure.

1 A finite element code for the analysis of damped cable system

A basic Finite Element (FE) code was defined to analyse frame structures incorporating damped cable (DC) systems, since only a very simplified model, characterised by notable computational limitations (shear-type schematisation of frames; only beam and column elements included in the library of the program; modal analysis only provided for bare frame configurations; etc) was available at the beginning of this research.
The main analytical and algorithmic features of the new code, as well as its capabilities at the current stage of development, are described in the following sections.

1.1 Model description

1.1.1 Hypotheses and limitations

The model is based on the following hypotheses and limitations:

- the behaviour of cable is linear;
- damper response is non-linear visco-elastic;
- friction effects between cable and slabs are neglected, thus cable force is constant along stories;
- vertical forces generated by cables are neglected;
- foundation and ground displacements coincide ($u_t = u_0$)

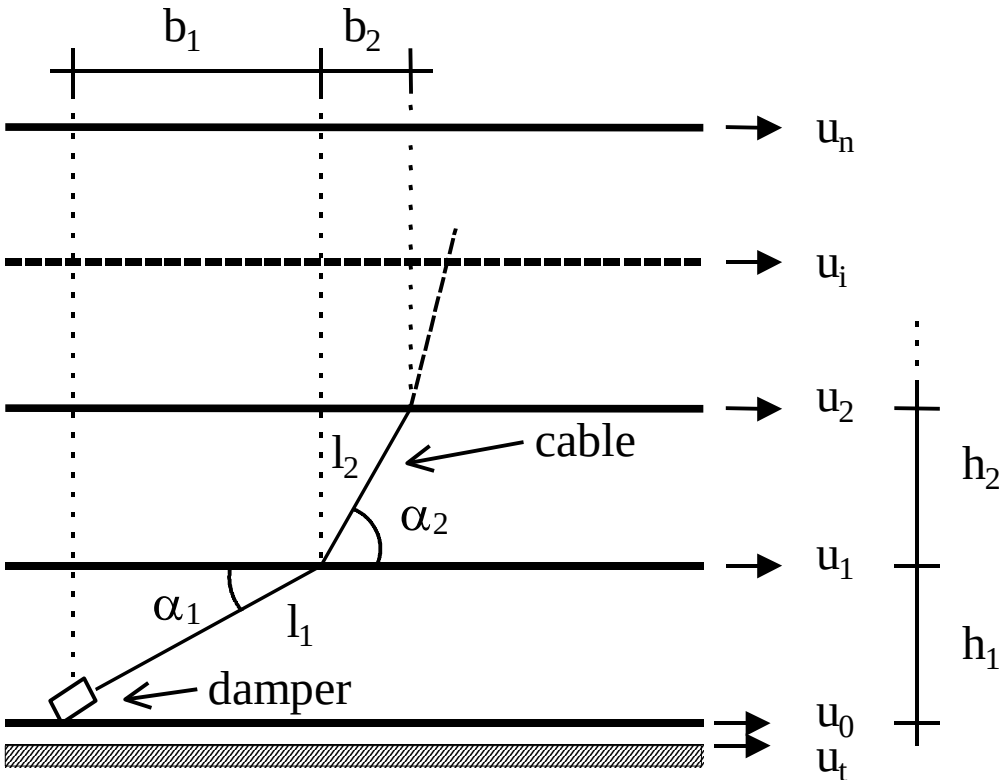

1.1.2 Cable stretch

Symbols used to denote cable lengths are given in the following table:

	Undeformed	***Deformed***
1.1.1.1.1 Total length	l_0 $l_{0,i}$ $b_{0,i}$	l l_i b_i
1.1.1.1.1.1 Length (floor i *)*		
1.1.1.1.1.1.1 Projection (floor *i*)		

Total cable length is given by:

$$l = l(u_i) = \sum_{i=1}^{n} l_i$$

1.1.1.1.1.1.1.1 Inter-story drift is equal to:

$$u_i - u_{i-1} = b_i - b_{0,i} = \Delta b_i$$

Thus cable length at *i*-th interstory becomes:

$$l_i = \sqrt{b_i^2 + h_i^2} \cong l_{0,i} + \Delta b_i \cdot \cos\alpha_i$$

Total cable length is:

$$l = \sum_{i=1}^{n} l_i = l_0 + \sum_{i=1}^{n} \Delta b_i \cdot \cos\alpha_i$$

Therefore cable stretch depends only on story displacements

$$\eta = \frac{l - l_0}{l_0} = \frac{1}{l_0}\left(\sum_{j=0}^{n} u_j \left(\cos\alpha_j - \cos\alpha_{j+1} \right) \right)$$

with

$$\cos\alpha_0 = \cos\alpha_{n+1} = 0$$

1.1.3 Cable stiffness matrix

Total cable force is expressed as

$$T = T_0 + EA \cdot \eta \geq 0$$

where T_0 is cable prestress force. As shown in the following figure, action of cable on *i*-th slab is given by

$$F_i = T \cdot (\cos\alpha_i - \cos\alpha_{i+1})$$

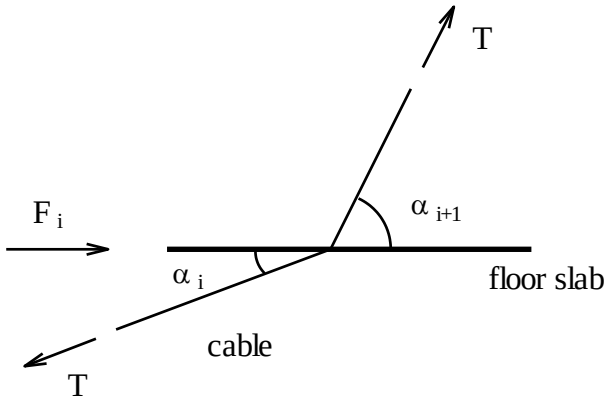

As F_i linearly depends on floor displacements u_j, cable stiffness matrix can be evaluated as follows:

$$K_{ij} = \frac{\partial F_i}{\partial u_j} = \frac{EA}{l_0} \cdot (\cos\alpha_i - \cos\alpha_{i+1}) \cdot (\cos\alpha_j - \cos\alpha_{j+1})$$

1.1.4 Damper contribution

Jarret fluid-viscous damper can be modelled as the ensemble of a spring and a viscous damper placed in parallel:

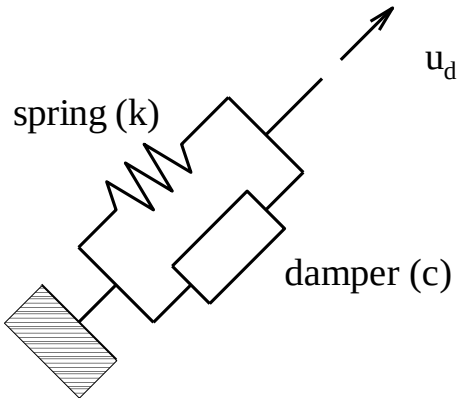

The action of damper:

$$F_d(u_d, \dot{u}_d) = F_k(u_d) + F_c(\dot{u}_d)$$

is non linear in terms both of displacement and speed.

Spring response is modelled by a bilinear scheme:

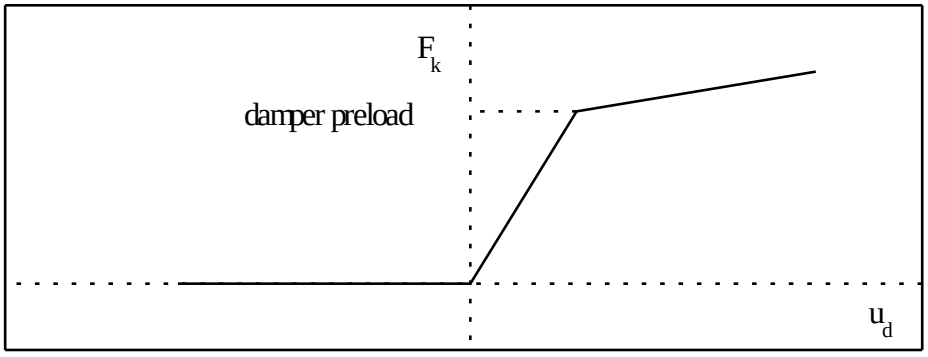

Viscous force is characterised by the following relationship:

$$F_c(\dot{u}_d) = c_d \cdot |\dot{u}_d|^{\alpha} \cdot \mathrm{sgn}(\dot{u}_d)$$

demonstratively sketched in the subsequent figure for a α value belonging to the typical range [0.1 – 0.2], that qualifies this class of dissipaters.

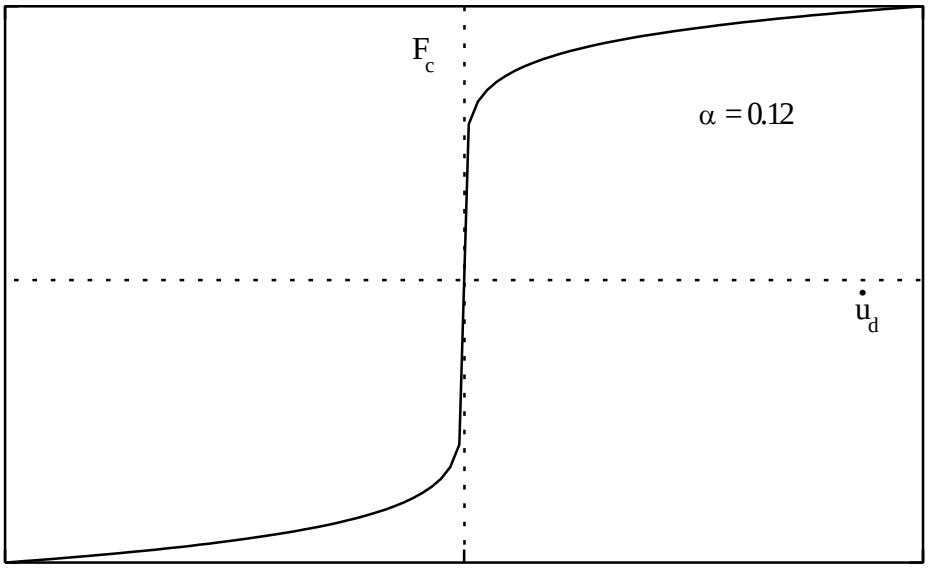
F_c
$\alpha = 0.12$
$\dot{u}_d$

1.2. Nonlinear dynamic analysis

1.2.1 Dynamic equilibrium equation

In order to perform time integration, Newmark implicit method was chosen as the reference algorithm. At each time t, the unknown displacement vector $u^{t+\Delta t}$ is searched by imposing equilibrium at time t+Δt (Δt being the time step assumed in the analysis):

$$F = F_I + F_C + F_K - R = 0$$

where:

- F_I = inertia forces;
- F_C = damping forces;
- F_K = elastic forces;
- R = external forces.

After some elaboration, dynamic equilibrium equation can be written as:

$$F = K' u^{t+\Delta t} + F_K'\left(u^{t+\Delta t}\right) + F_C'\left(\dot{u}^{t+\Delta t}\right) - R' = 0$$

where:

- K' = generalised stiffness matrix;
- F'_K = non-linear elastic forces;
- F'_C = non-linear viscous forces;
- R' = generalised external forces.

Therefore, at each step of the process are to be found the displacement vector $u^{t+\Delta t}$ and the related speed vector that satisfy dynamic equilibrium equation $F = 0$. Because of the strong non-linearity of damping forces, a simple Newton-Raphson technique is not sufficient to achieve convergence; thus it is necessary to couple it with a line-search algorithm, as described in [1].

1.2.2 Newton-Raphson method with line-search

The idea is to solve non-linear equation F=0 by minimising the following function:

$$g(u^{t+\Delta t}, \dot{u}^{t+\Delta t}) = \frac{1}{2} F \cdot F$$

This is accomplished by moving along the descent direction Δu given by Newton-Raphson method

$$\Delta u_i = - J^{-1}(F)\Big|_{u_i} \cdot F$$

by an optimal step size λ_i found with a line-search algorithm

$$u_{i+1} = u_i + \lambda_i \cdot \Delta u_i$$

Obviously, $0 < \lambda_i \leq 1$; when $\lambda_i = 1$, original Newton-Raphson algorithm is obtained.

Such a method belongs to the class of globally convergent method, and proved to be very effective in finding dynamic equilibrium solution for each time step. It should nevertheless be noted that:

- viscous force function must be smoothed near origin, so as to avoid that its derivative goes to infinity;
- the time step Δt must be chosen with care;
- secant stiffness and damping coefficient values are to be preferred to tangent ones.

1.3 Finite Element code

The finite element engine was developed with the following design targets:

- static, modal and direct dynamic analysis (linear and non-linear):
- analysis of 2D frames with beams, columns and shear walls;
- easy extension to 3D structures;
- suited for parametric analysis;
- fast and compact.

The code architecture is described in the following figure:

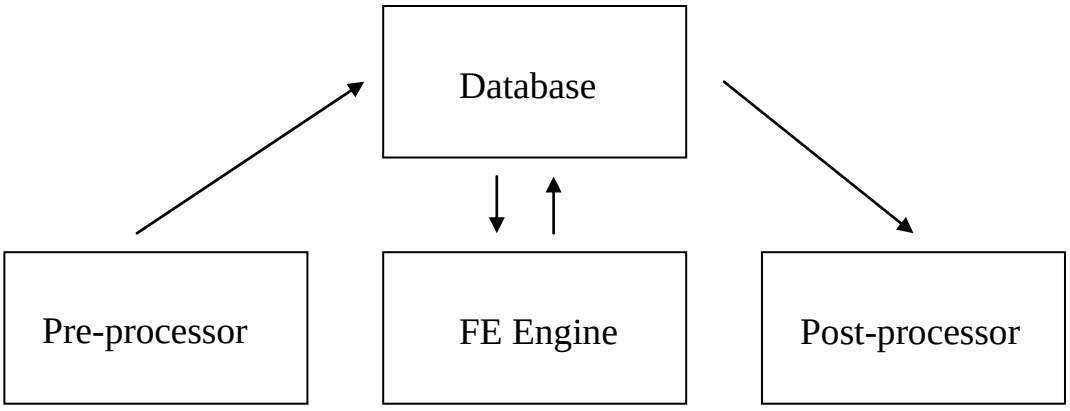

Pre-processing is done by an ASCII file parser that in future versions may be replaced by a graphical interface; post-processing consists also of an ASCII file in tabular form suited to be loaded into a spreadsheet application. Present version of code, developed in ANSI C++, is completely object-oriented and design-patterns based in order to improve extendibility and reusability. Some FORTRAN libraries were used for computational-intensive routines.

1.4 Conclusive remarks

The damped cable system can effectively be modelled as an “ordinary” finite element, although non-linearity must be treated with care to achieve convergence. Algorithms and code proved to be stable, scalable and fast for parametric analysis.

1.5 Future extensions

Future development directions include the following targets:

- improvement and extension of DC model, and its tuning against experimental results;
- extension of FE model to 3D structures;
- optimisation of time-integration algorithms;
- replacement of ASCII file parser with graphical interface.

1.6 Bibliography

[1] Numerical Recipes in C: The Art of Scientific Computing, Cambridge University Press, 1988-1992, available online at http://www.nr.com/.

2 First series of mock-up analyses

2.1 Geometry of structure

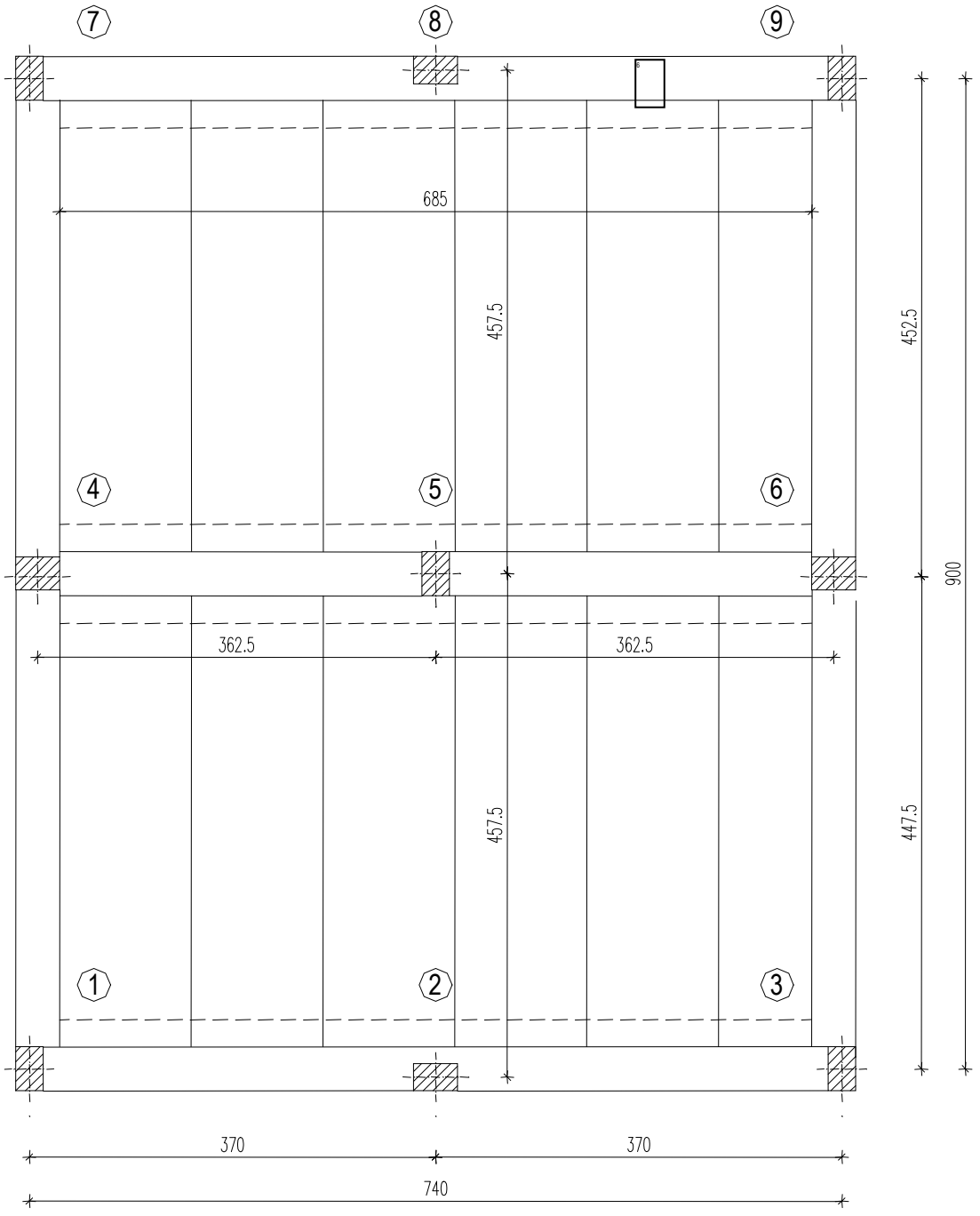

2 First floor plan (dimensions in meters)

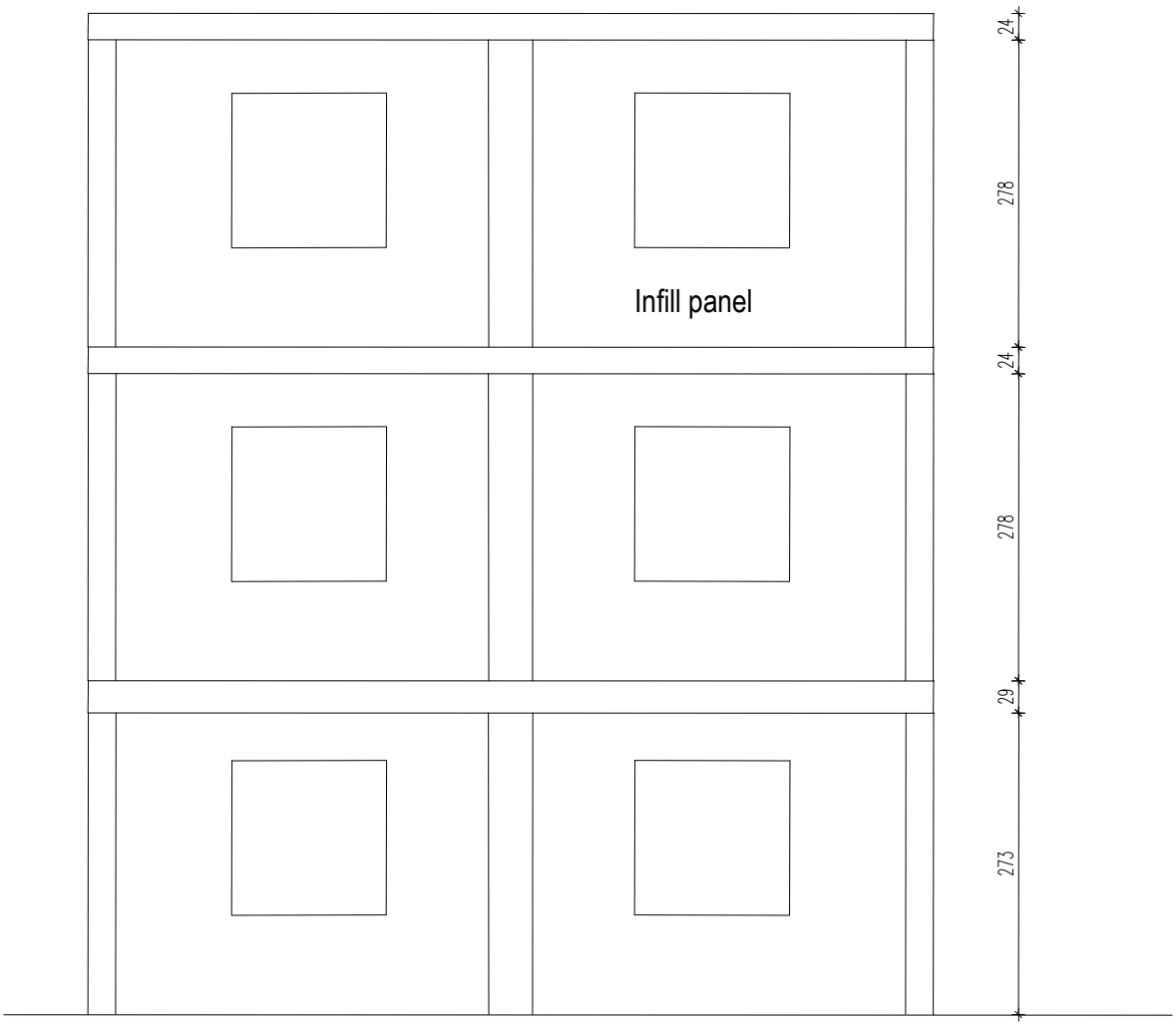

3 North view (dimensions in meters)

2.2 Materials

Materials used in mock-up building are:

Material	Used for:
Reinforced concrete	Beams, Columns
Bricks	Infill panels

2.3 Beam and column cross sections

The dimensions of beam and column cross sections are (dimensions in centimetres):

Story	Beams 1-3, 7-9	Beam 4-6	Beams 1-7, 3-9	Beam 2-8
1	65 x 24	90 x 24	40 x 24	==
2	65 x 12 + 40 x 12	100 x 12 + 50 x 12	40 x 24	==

3	65 x 24	90 x 24	40 x 24	180 x 24

3.1 Story	**Columns 1-3-7-9**	**Columns 2-8**	***3.2 Column 4-6***	**Column 5**
1	25 x 40	40 x 25	40 x 30	25 x 40
2	25 x 40	40 x 25	40 x 30	25 x 40
3	25 x 40	40 x 25	40 x 30	25 x 40

2.4 Load analysis

Story	**Floor own loads [KN/m^2]**	**Permanent loads [KN/m^2]**	**Live loads [KN/m^2]**
1	3.4	2.0	2.0
2	2.7	2.0	2.0
3	2.7	1.5	1.2

2.5 Finite element model

As the finite element code developed at this stage can model only two-dimensional structures, mock-up building has been analysed in the East-West direction by putting frames 1-3, 4-6, and 7-9 in series. Infill panels have been modelled with "ad hoc" shell elements with proper stiffness.

It should be noted that this preliminary investigation has been conducted by referring to the mechanical characteristics of the virgin structure (i.e., before the development of the damaging experimental campaigns), as well as for infill panels extended over the entire height of the building. The aim of this enquiry was in fact to prepare a complete 2D model (incorporating infills) capable of reproducing the actual dynamic properties and test loading action for any possible initial condition of the mock-up. This will allow to carry out the final analyses once all precise data concerning the *actual* initial conditions, to be attained by means of a proper identification survey on the repaired building, will be available.

2.5.1 Modal analysis

Consistently with previous observation, modal analysis was conducted for demonstrative comparison with the experimentally measured periods in virgin conditions. The following results were obtained by means of proper choices of the R/C element properties, and reasonable assumptions about the infill panel ones:

Mode	**Numerical result [Hz]**	**Measured result [Hz]**
1	8.01	7.74
2	27.20	26.80

3.2.1.1.1 If desired, it is obviously possible to further calibrate the model so as to reach total superposition of results.

2.5.2 Dynamic analysis

Forces

Vibrodyne action has been simulated by a sinusoidal force applied to the upper floor, intensity and frequency of which are summed up in the diagrams reported below.

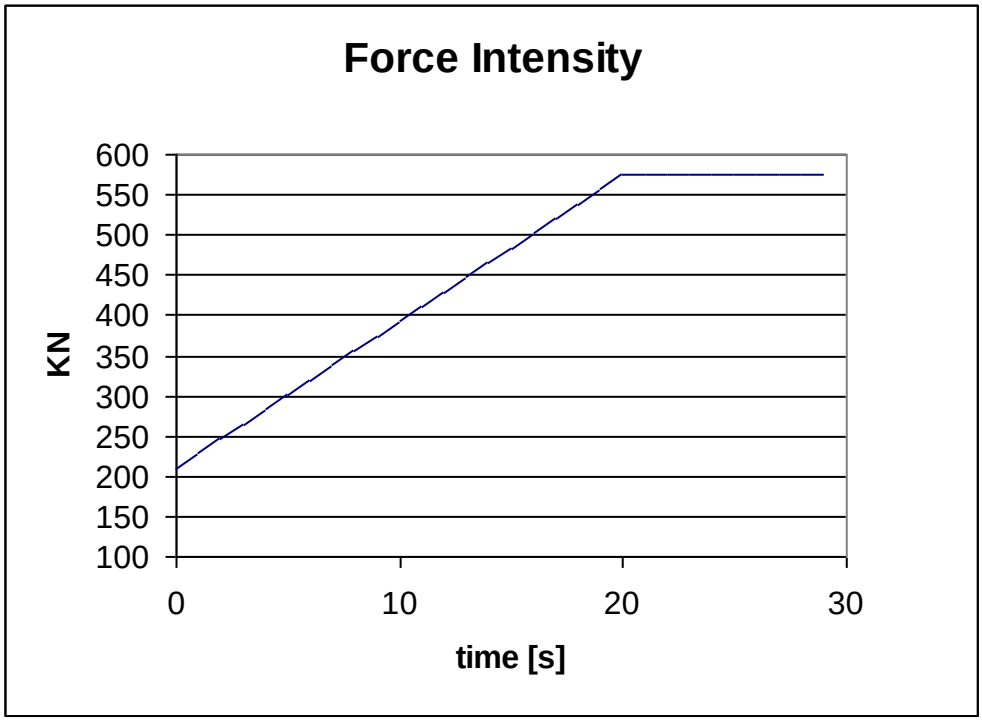

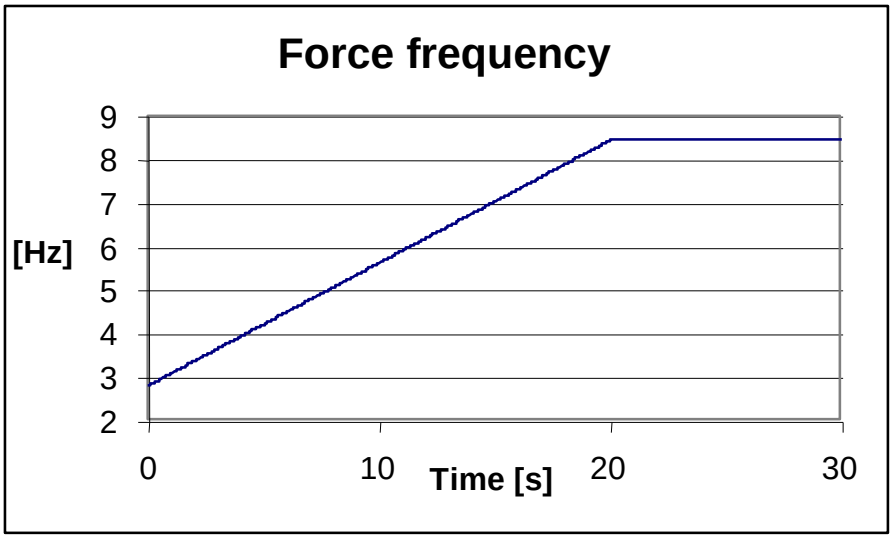

3.2.2

3.2.3 Cables

Two couples of cables were applied on frames 1-3 and 7-9, respectively; the following parameters were used in computations:

- Damper viscous coefficient c 100 kN;
- Damper stiffness k_1 4500 MN/m;
- Damper stiffness k_2 2.5 – 5.0 – 10.0 MN/m,

as well as the following combination of cable area and damper preload:

Cable area [mm^2]	Damper preload [kN]
1050	185
1050	350
1050	440
1050	600
1800	185
1800	350
1800	440
1800	600

3.2.4 Results

Cable area of 1050 mm^2 proved to be sufficient to limit storey displacements, with notable improvements of response performance compared to un-protected building (anyhow decidedly stiffened by the effect of infill panels), as shown in the diagram traced out below. An adequate preload (> 350 KN) is moreover necessary in order to avoid cable compression.
Final tuning of damped-cable parameters will be possible when all needed information on the actual mock-up mechanical characteristics will be available.

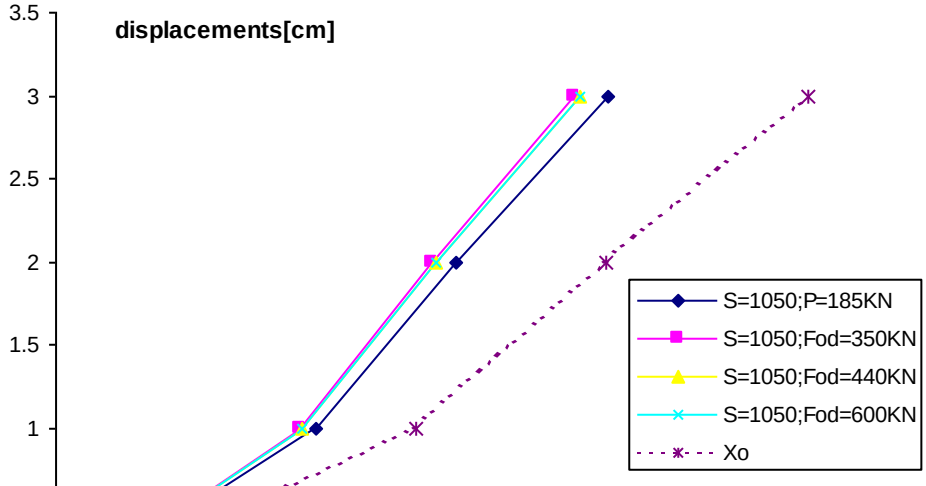

3 Param

3.1 Aim o

Distinctive) system have
been highl
The role o

- cable layout;
- cable pre-tension (named F_{oc});
- damper pre-load (F_{od});
- cable section (S_c);
- viscous damping coefficient (C);
- upper anchorage level.

Effectiveness of seismic protection has been evaluated by referring to the following effects on structural response:

- importance of higher mode contribution;
- reduction of story shears and interstorey drifts;
- reduction of storey displacements.

3.1.1 Input ground motions

Two series of four artificial accelerograms were used as input, both generated from EC8 response spectrum by assuming soil type A, and $a_{max}/g=0.35$ (Fig. 3.1.1). The first series was jointly calibrated on the "Italian Guidelines for isolated structures", which determined a highly engaging demand on structures analysed. Signals belonging to the second group are characterised by a shorter duration, nearer to the one of real events.

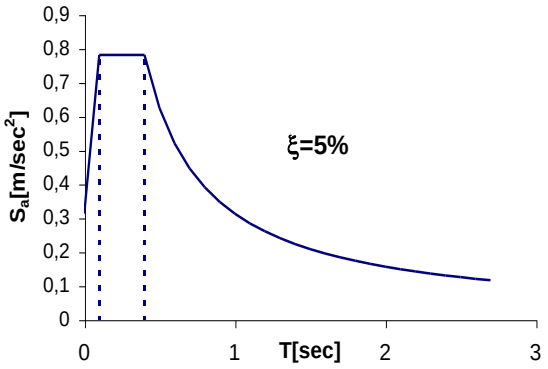

Fig. 3.1.1. EC8 response spectrum scaled to the peak ground acceleration

In order to assess the damage potential of accelerograms selected for numerical analyses, the well-known Arias and Housner indexes, both giving a measure of input energy, were basically utilised:

$$I(Arias) = \frac{\pi}{2g}\int_0^{t_d} \ddot{v}_g{}^2 dt$$

$$I(Housner) = \frac{1}{t_{0.95} - t_{0.05}}\int_{t_{0.05}}^{t_{0.95}} \ddot{v}_g{}^2 dt$$

where

$\ddot{v}_g$ = ground acceleration;

t_d = duration of seismic event;

$t_{0.05}$ = time at which 5% of Arias integral is covered;

$t_{0.95}$ = time at which 95% of Arias integral is covered.

A third index, derived from the Arias one, was also considered:

$$PD = \frac{I(Arias)}{\nu_o^{\,2}}$$

where

$\nu_o = \frac{n}{t_d}$;

n=number of sign changes.

Concerning *PD*, recently introduced for seismic ground motion classification, it can observed that its highest values are generally associated with the highest ductility demands on structures.
The following results were obtained by applying the three operators:

FIRST SERIES

Duration: 35 seconds; *Stationary part: 25 seconds*

	ACL1_1	*ACL1_2*	*ACL1_3*	*ACL1_4*
I(Arias)	9.84	10.24	11.63	10.8
I(Housner)	1.71	1.84	2.12	1.95
ν_o	17.8	18.65	18.48	19.22
PD	0.034	0.031	0.036	0.03

SECOND SERIES

Duration: 25 seconds; *Stationary part: 15 seconds*

	ACL2_1	*ACL2_2*	*ACL2_3*	*ACL2_4*
I(Arias)	7.7	7.4	8.14	7.58
I(Housner)	1.97	1.84	2.07	1.96
ν_o	18.16	18	17.6	18.64
PD	0.023	0.022	0.028	0.023

3.1.2 Case study structures

Three buildings designed only for vertical loads, and two structures seismically designed by conforming to EC8 rules (with reference to the scaled spectrum in Fig. 3.1.1), respectively sketched in Fig. 3.1.2 and 3.1.3 (where the fundamental vibration period T_1 values are also reported), were assumed as basic case studies for the numerical investigation.
A second 4-storey building, with the same geometrical dimensions of the first one, but seismically designed (for which T_1=0.35 s), was also analysed.

4-storey building

T_1 = 0.7 s

(T_1= 0.35 s for seismically designed version)

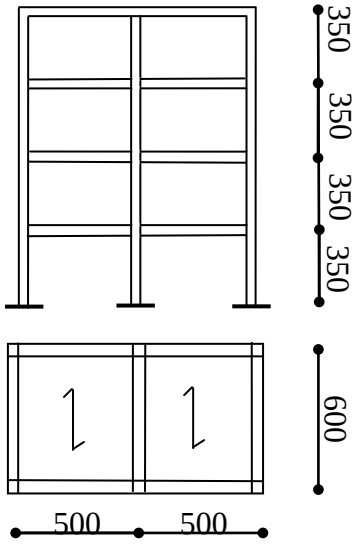

8/10-storey buildings

T_1 = 1.24 s (8)

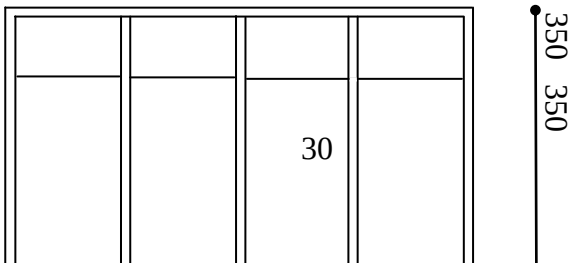

T_1 = 1.41 s (10)

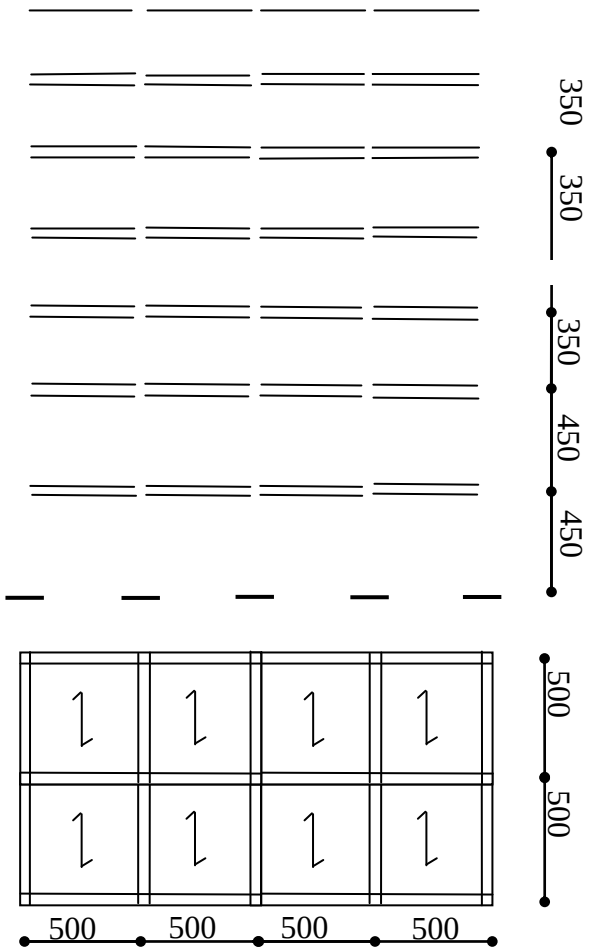

Fig. 3.1.2. Non-seismically designed case study buildings

EC8 frame structure

T_1 = 0.82 s

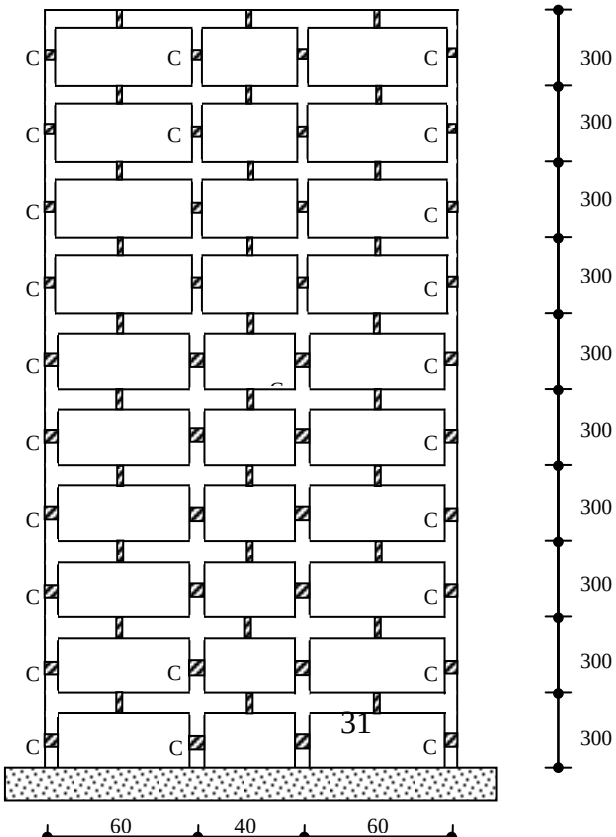

EC8 dual structure

T_1 = 0.62 s

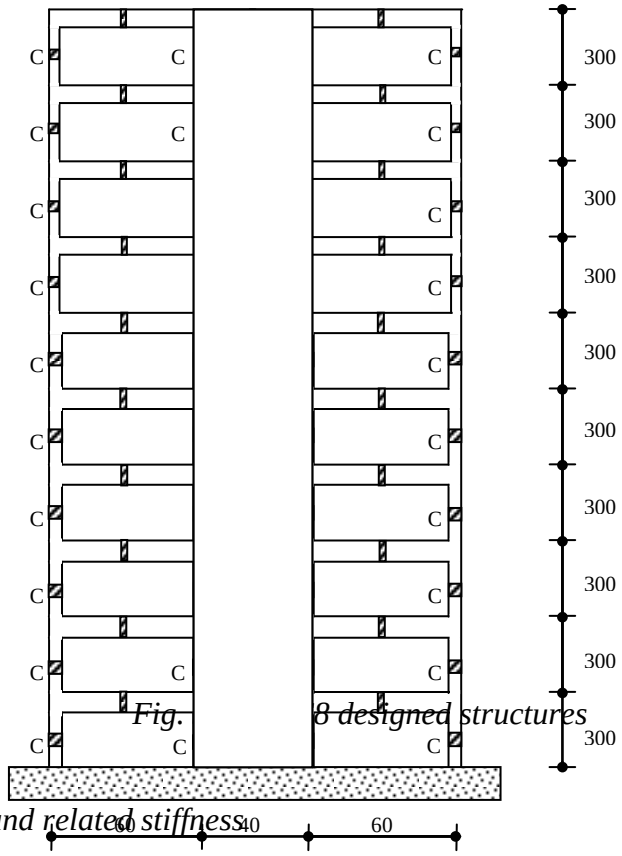

Fig. 8 designed structures

3.1.3 Cable layout

Evaluation of layout and related stiffness

Cable was modelled as an axial force-resisting element, with axial force F constant along its length L (this last being dependent on layout assumed). Cable stiffness is expressed in the form:

$$K_c = \frac{ES}{L}$$

where E is the Young modulus.

By considering in detail a zone comprised between two subsequent storeys (Fig. 3.1.4):

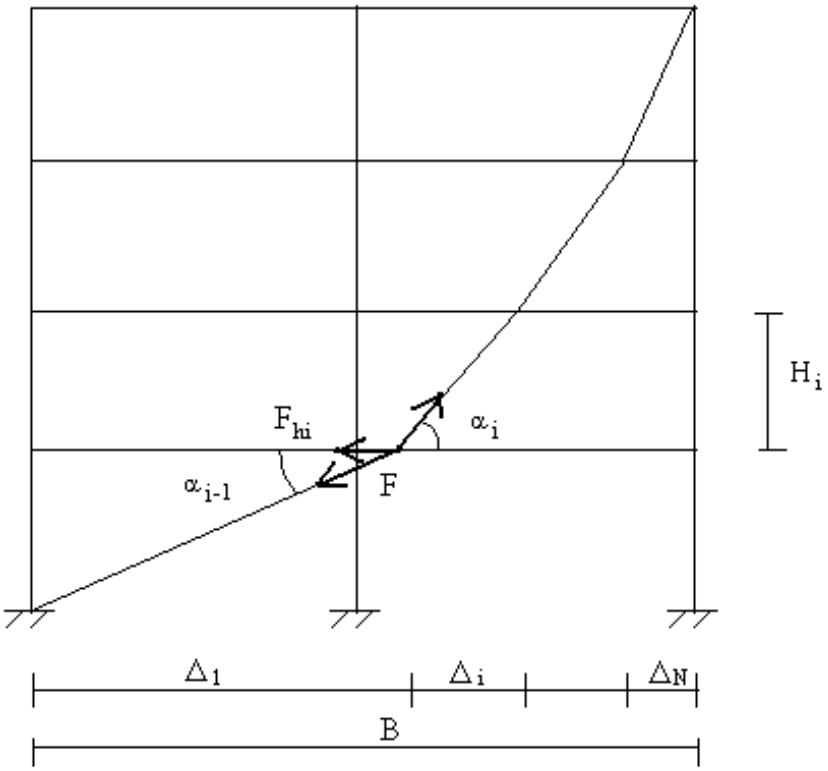

Fig. 3.1.4. Cable layout

the elements of cable stiffness matrix (see section1) can be expressed as:

$$K_{ij} = \frac{dF_i}{du_j} = \frac{EA}{l_o}(\cos\alpha_i - \cos\alpha_{i+1})(\cos\alpha_j - \cos\alpha_{j+1})$$

Numerical analyses were focused on the following cable configurations:

- layout with "constant horizontal forces"→"CHF";
- polynomial of orders 2, 3 and 4;
- diagonal.

"CHF" layout

This configuration gives rise to the same reaction forces F_{Hi} at each level. By assuming that the angle α between cable and slabs does not change after deformation, the characteristics of this layout are defined by the relations reported below (where B is the distance between the extremities of cable measured on the horizontal axis; N is the total number of storeys; H_i is the *i*-th storey height; and Δx_i is the horizontal projection of cable in correspondence with the *i*-th storey — Fig. 3.1.4):

$$\begin{cases} \dfrac{F}{F_{H,n}} = \cos\alpha_n = A = const \\ \dfrac{F}{F_{H,n-1}} = \cos\alpha_{n-1} - \cos\alpha_n \rightarrow \cos\alpha_{n-1} = 2A \\ \ldots \\ \ldots \\ \dfrac{F}{F_{H,1}} = \cos\alpha_1 - \cos\alpha_2 \rightarrow \cos\alpha_1 = nA \end{cases}$$

From these relations, it follows that: $\cos\alpha_1 = n\cos\alpha_n = nA$. Furthermore:

$$B = \sum_{i=1}^{n} \Delta x_i = \sum_{i=1}^{n} \frac{H_i}{\left[\dfrac{1}{(n-i+1)^2 A^2} - 1\right]^{1/2}}$$

A non-linear problem is thus obtained, which can be solved using the iterative solution scheme reported in the next page. At the end of the process the unknown values Δx_i are obtained.
Condition $\cos\alpha_i = (n\text{-}i+1)A$ underlines that the higher stiffening effects are generated at the lower levels, i.e., the ones providing the greatest $(\cos\alpha_i - \cos\alpha_{i+1})$ and $(\cos\alpha_j - \cos\alpha_{j+1})$ contributions.

Polynomial layouts

Polynomial layouts of order n are defined by the corresponding analytical curves with zero slope at the origin; the higher n, the lower the angle α at the base, and the quicker the α growth with height (for $n \geq 4$, nearly vertical slopes are obtained at the top).
As a consequence, very low K_{ij} values are found for the highest floors also in this case.

Diagonal layout

For this configuration α does no vary with height; the only non-zero K_{ij} terms are derived at the top storey, related to the total displacement at this level.

$$\frac{B}{\sqrt{H_{tot}^{\ 2} + B^2}} = \cos\alpha_{\min}$$

$$\frac{B}{\qquad} = \cos\alpha$$

$$\cos\alpha_1 = \frac{\cos\alpha_{\min} + \cos\alpha_{\max}}{2}$$

$\cos\alpha_{\max} = \cos\alpha_1$
(the highest value for α_1 is reduced)

$\cos\alpha_{\min} = \cos\alpha_1$
(the minimum value for α_1 is raised)

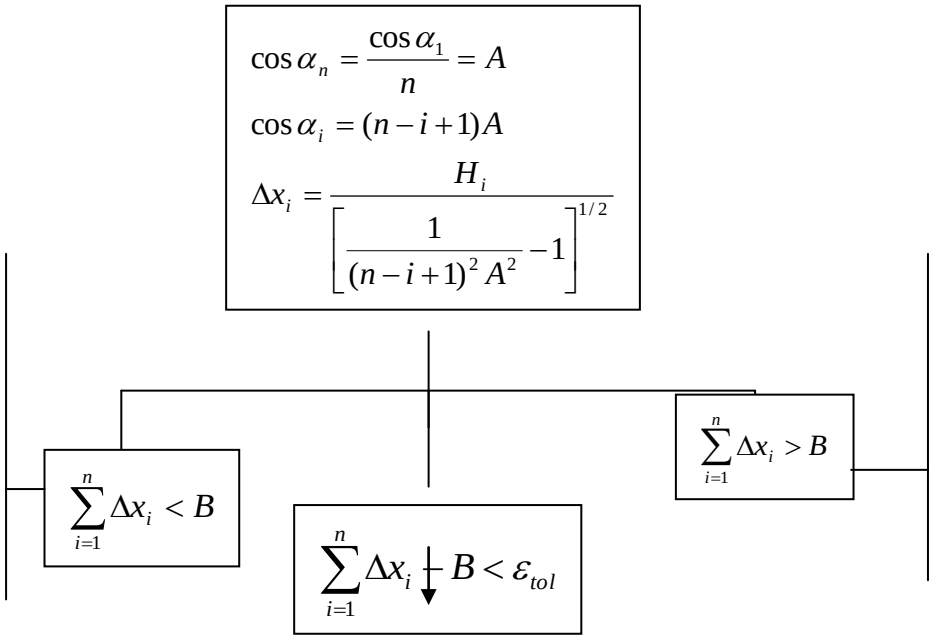

3.1.4 Vibration modal shapes

As way of example, periods (T_i) and load participation factors (L) of the bare 8-storey building are presented:

mode	*1*	*2*	*3*
T_i [s]	1.24	0.38	0.23
L [%]	84	8.3	4.7

The relevant eigenvectors are shown in Fig. 3.1.5.
The same parameters are analysed in the presence of the damped cable system, for different layouts, by fixing the cable section S_c at 5700 mm^2 (which corresponds to two cables of seven strands plus two cables of twelve strands). Cable abscissas of intersections with floors are reported below, whereas a graphical representation of cable configurations considered is traced out in Fig. 3.1.6.

		Diag.		**CHF**		**Pol2**		**Pol3**
storey		*X[m]*		*X[m]*		*X[m]*		*X[m]*
1		3		6.5		7.65		10.54
2		6		11.25		10.9		13.34
3		8.33		14.03		12.87		14.91
4		10.67		16.15		14.58		16.20
5		13		17.75		16.11		17.31
6		15.33		18.89		17.5		18.30
7		17.67		19.63		18.79		19.19
8		20		20		20		20

Eigenvalues and load participation factors L_i have been calculated for two different hypotheses concerning the stiffness of first and second branches of damper constitutive relationship:

(a) K_{d1}=122 MN/m, K_{d2}=6.1 MN/m;
(b) K_{d1}=4500 MN/m, K_{d2}=3 MN/m.

(a1) K_{d1}=122 MN/m

	Diag.			**CHF**			**Pol2**			**Pol3**		
mode	*1*	*2*	*3*	*1*	*2*	*3*	*1*	*2*	*3*	*1*	*2*	*3*
T [s]	0.67	0.32	0.22	0.56	0.37	0.23	0.63	0.38	0.21	0.71	0.38	0.21

L [%]	89	0	8	68	20	8	78	7	11	72	12	11

(a2) K_{d2}=6.1 MN/m

	Diag.			**CHF**			**Pol2**			**Pol3**		
mode	*1*	*2*	*3*	*1*	*2*	*3*	*1*	*2*	*3*	*1*	*2*	*3*
T [s]	0.93	0.37	0.23	0.91	0.38	0.23	0.95	0.38	0.23	1	0.38	0.23
L [%]	87.5	4.6	5.4	82	10	5	83	8	6	81	9	6

(b1) K_{d1}=4500 MN/m

	Diag.			**CHF**			**Pol2**			**Pol3**		
mode	*1*	*2*	*3*	*1*	*2*	*3*	*1*	*2*	*3*	*1*	*2*	*3*
T [s]	0.65	0.31	0.22	0.52	0.37	0.23	0.6	0.38	0.21	0.68	0.38	0.21
L [%]	89	0	9	61	25	10	76	6	13	69	12	11

(b2) K_{d2}=3 MN/m

	Diag.			**CHF**			**Pol2**			**Pol3**		
mode	*1*	*2*	*3*	*1*	*2*	*3*	*1*	*2*	*3*	*1*	*2*	*3*
T [s]	1.04	0.37	0.23	1.02	0.38	0.23	1.05	0.38	0.23	1.09	0.38	0.23
L [%]	86	6	5	83	9	5	84	8	5	83	9	5

The relevant eigenvectors are drawn in Figs.3.1.7÷10.
The following main observations emerge from these data:

a. negligible differences between (a1) and (b1) come out, due to the fact that K_{d1} is in both cases significantly higher than cable stiffness K_c;
b. only for a very high value of ratio K_{d1}/K_{d2} appreciable differences are noticed (a2 $\rightarrow$ b2);
c. first-mode eigenvector components are decidedly limited at the base, whereas tend to the bare frame ones at the upper floors;
d. although first mode factor dominates, higher modes contributions are never negligible;
e. for diagonal layout, a remarkable limitation of top displacements, causing high storey shears, is surveyed. As regards the remaining layouts, the effects of DC system on deformations are similar to the ones that could be induced by a partial-height shear wall; this is the consequence of the fast reduction of stiffening contribution provided by the cable along the vertical axis.

3.2 Influence of cable layout

Diagonal layout was analysed first within the dynamic enquiry carried out for the three non-seismically designed buildings (Figs. 3.2.1÷9 where, as for subsequent figures, the mean results over the ensemble of eight accelerograms are drawn), which confirmed its poor performance especially for the 8 and 10-storey systems. These last are in fact the most sensitive to the effect observed at point *e* of previous section. Irregular storey shear and displacement distributions were particularly noticed, with shear values higher than the ones calculated for the corresponding bare structure, at several levels, and inverted drifts in the upper floors.
CHF and Pol2 layouts provided the best balanced benefits in terms of shear and drift; even though lightly higher reductions of base shear are induced by Pol3 and Pol4, global control on deformation is less satisfactory (Figs. 3.2.10÷18) in these last cases. It must be underlined that all previous results are referred to the C values minimising base shear.
Again with this hypothesis, CHF layout was directly applied to EC8 frame structure, still assuming S_c = 5700 mm^2 (Figs.3.2.19÷22). Storey shear reductions ranging from 32% to 45% for the most engaged floors came out, with respect to bare frame conditions. Furthermore, interstorey drifts never exceeded 0.2% of relevant storey heights, which represents a very good performance under the 0.35 g peak input acceleration.
Clear benefits are induced by the same CHF layout also in the EC8 dual structure (Figs.3.2.23÷25), with about 50% storey shear reduction over the entire height of the frame part, and till to the seventh floor for the wall (little lower reductions are observed only at the three upper floors).

3.3 Influence of cable pre-tension F_{oc} and damper pre-load F_{od}

A tentative design value of pre-tension, which is aimed at keeping the cable in tension even under the most engaging phases of seismic response, can be obtained by means of the following empirical relation:

$$F_{oc} = K_c \frac{\Delta L_c}{2 \div 3}$$

where ΔL_c= cable stretch corresponding to the maximum displacements calculated for the bare structure under the reference input action.
Two F_{oc} values were established for the parametric enquiry by means of the above relation; afterwards, the following ratios of F_{od} damper preload to F_{oc} were analysed:
(a) $F_{od}= 2F_{oc}$
(b) $F_{od}= F_{oc}$
Figures 3.3.1÷7 essentially show that under hypothesis (a), results obtained for the 4-storey building do not depend on C coefficient. This is the consequence of the high stiffness value assumed, for which the damping action is practically not mobilized.
The opposite happens in case (b), which gives rise to a decidedly more satisfactory behaviour of protected system.
Similar results were obtained for all remaining structures, with a trend toward increased differences between the two hypotheses dealt with, for increasing numbers of floors.

3.4 Influence of damping coefficient C

As already observed, viscous damping plays a decisive role in reducing response quantities when pre-load F_{od} is equal to F_{oc}.
Once fixed this parameter, for each structure analysed a value of C capable of maximising the benefits of DC protective system in terms of storey shear as well as interstorey drift, was found (Figs.3.4.1÷6).
By summing up the outcome of the six case studies dealt with, a relatively narrow C range ([60÷100] KN/(m/s)$^{\alpha}$), based on value 0.12 assigned to the α exponent, emerged.

3.5 Influence of upper anchorage level

Selected results obtained for the 8 and 10-storey buildings about the effects of upper anchorage level (i.e., when this does not coincide with the top floor) are presented, as way of example, in Figs.3.5.1÷3.
Due the varied horizontal projection of the cable, slightly decreased shear values were surveyed at the lower storeys compared to the ones provided by the basic configuration, and slightly increased values at the upper storeys.
Worse performance in terms of drifts were on the other hand obtained by lowering the anchorage level.

3.6 Cable section S_c

To complete parametric analysis, cable section was varied for the 4 and 8-storey buildings over a wide interval (600÷9300 mm^2), derived by proper combinations of the basic units constituted by 7 and 12 strands, as reported in the following table:

Sc (mm^2)	*m(7 strands)*	*p(12 strands)*
1050	1	0
1800	0	1
2100	2	0
3600	0	2
5700	2	2
9300	2	4

The results drawn in Figs.3.6.1÷2 show that for these two structures the optimal sections are 2100 mm^2 and 5700 mm^2 (i.e., the ones fixed during the previous phases of numerical enquiry), capable of minimising shears and drifts as well as of providing a rather uniform distribution of both quantities along the height.
Greater sections decrease storey displacements but, by increasing stiffness, they promote higher modes contribution, and thus more irregular response.
The 4-storey seismically designed building was also analysed under this viewpoint, showing that only very large sections (however over-dimensioned in comparison with benefits induced) give rise to non negligible effects (Figs.3.6.3÷4). This is the consequence of the high

stiffness of this building, which substantially reduces the effects of damper action on global structural response.

8-storey building

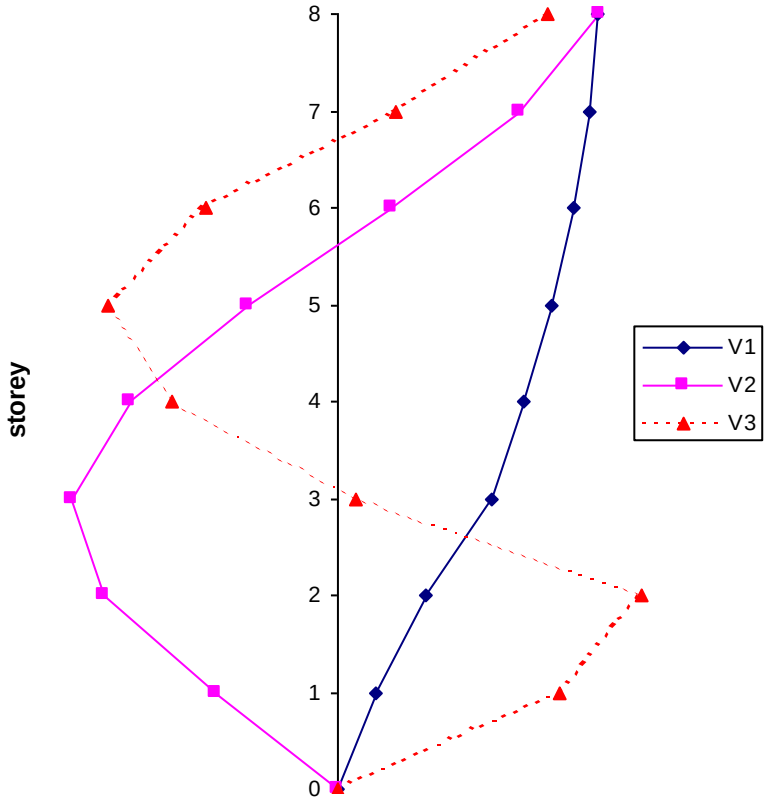

Fig. 3.1.5. Original structure: first three vibration modes.

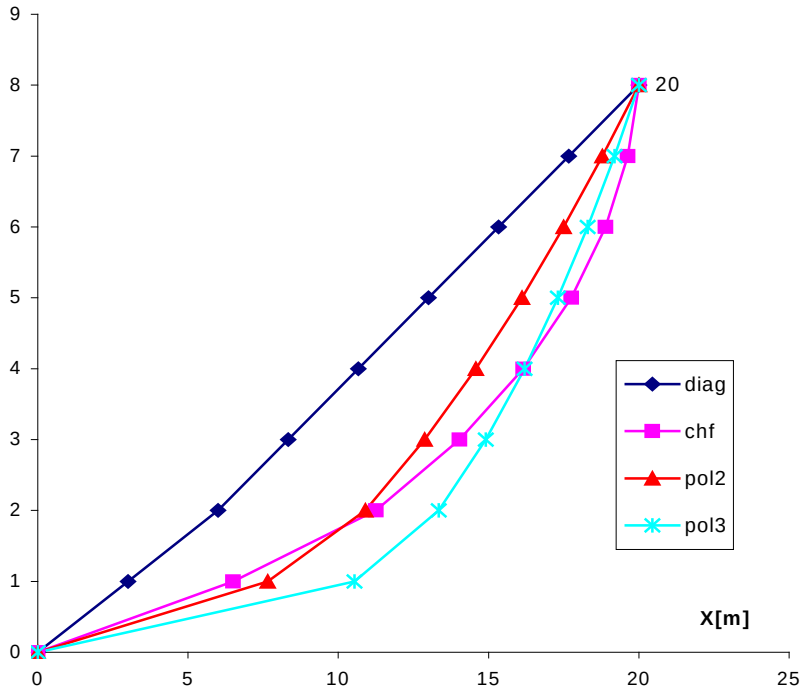

Fig. 3.1.6. Cable layouts.

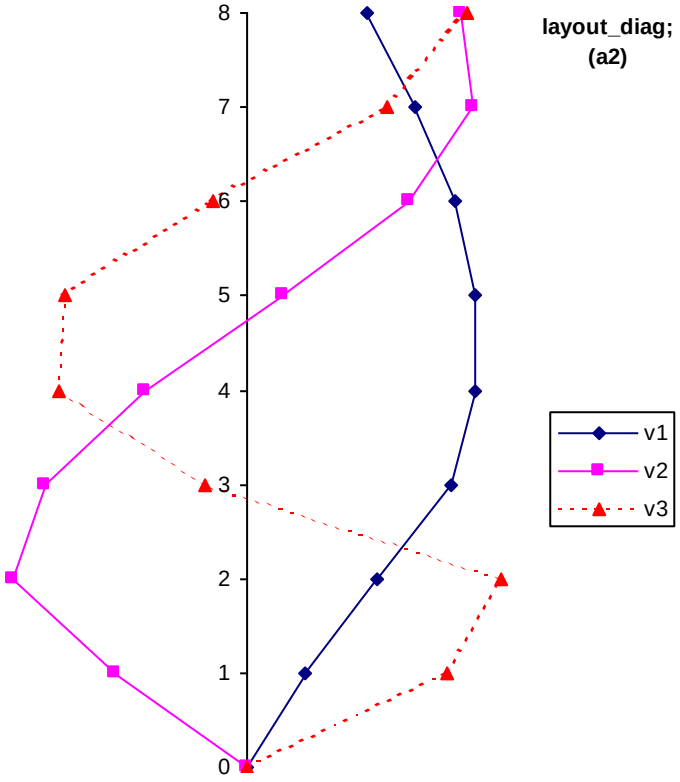
layout_diag;
(a2)
8
7
6
5
4
3
2
1
0
v1
v2
v3

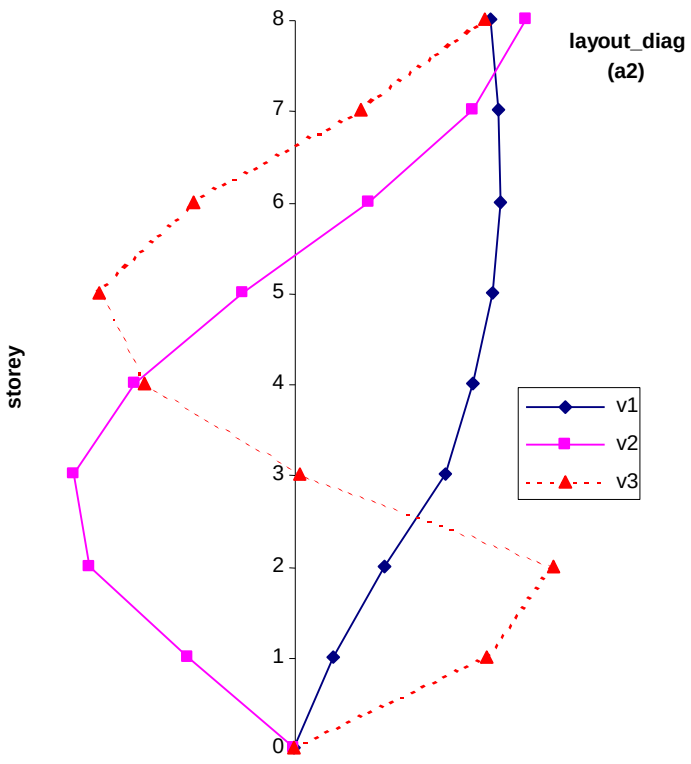
storey
layout_diag
(a2)
8
7
6
5
4
3
2
1
0
v1
v2
v3

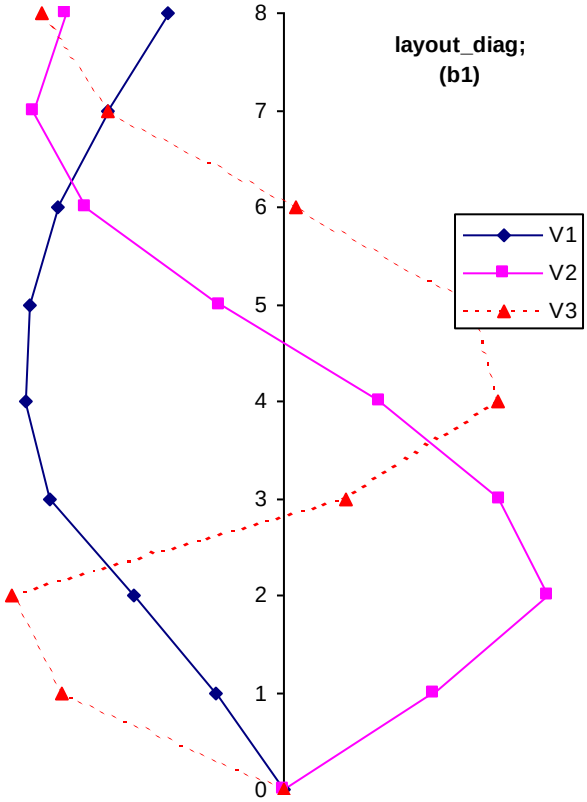
layout_diag;
(b1)
8
7
6
5
4
3
2
1
0
V1
V2
V3

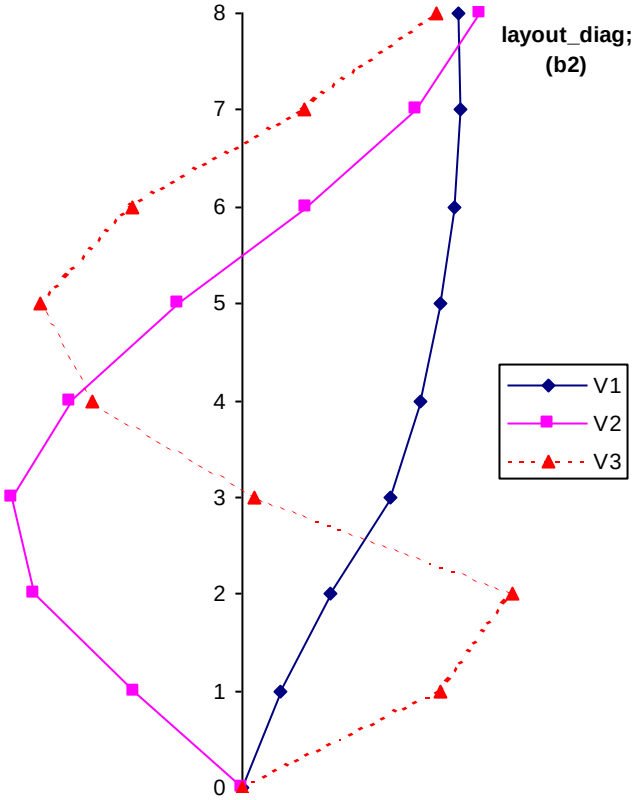
layout_diag;
(b2)
8
7
6
5
4
3
2
1
0
V1
V2
V3

Fig. 3.1.7. Diagonal layout: eigenvectors.

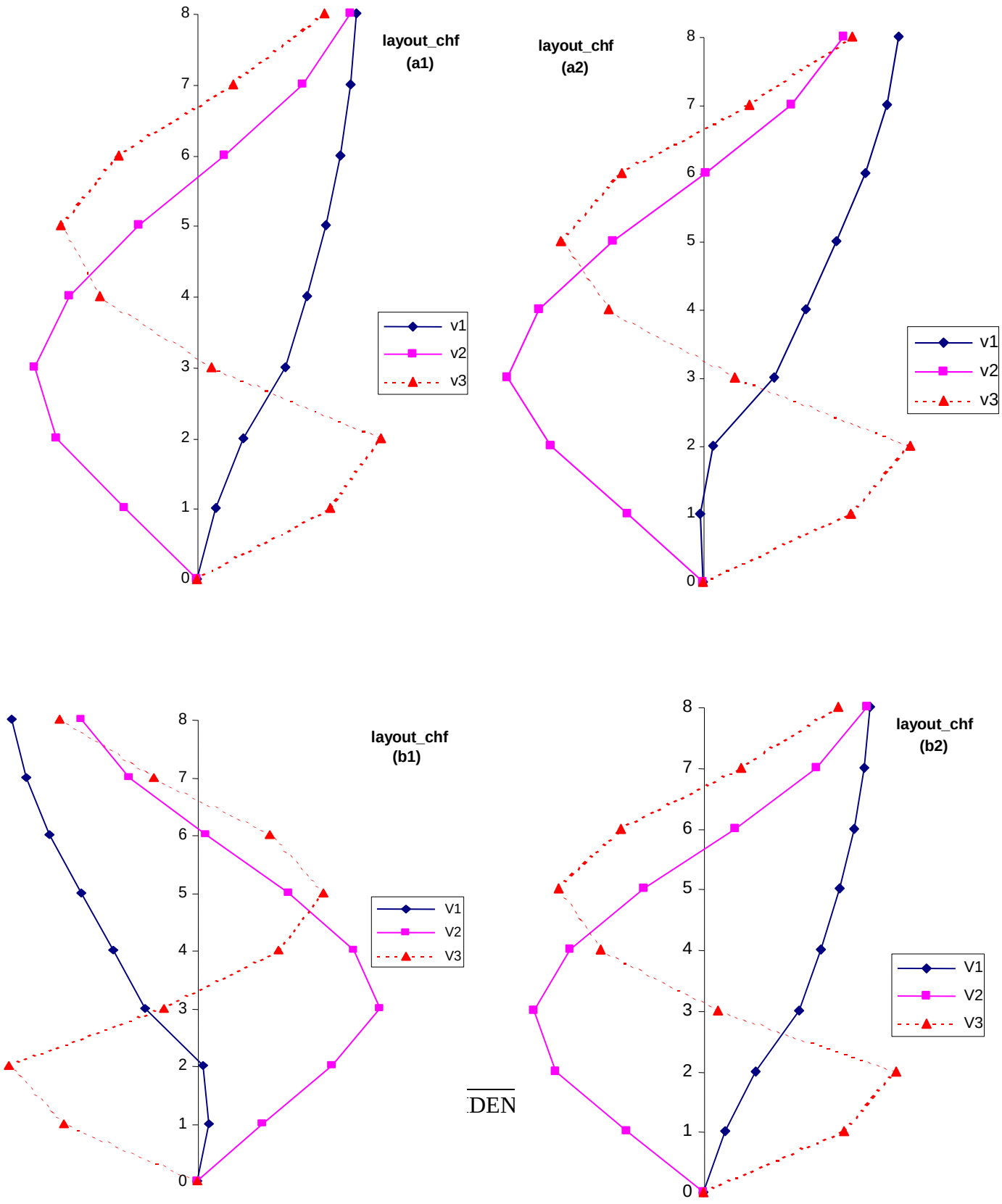

DEN

Fig. 3.1.8. CHF layout: eigenvectors.

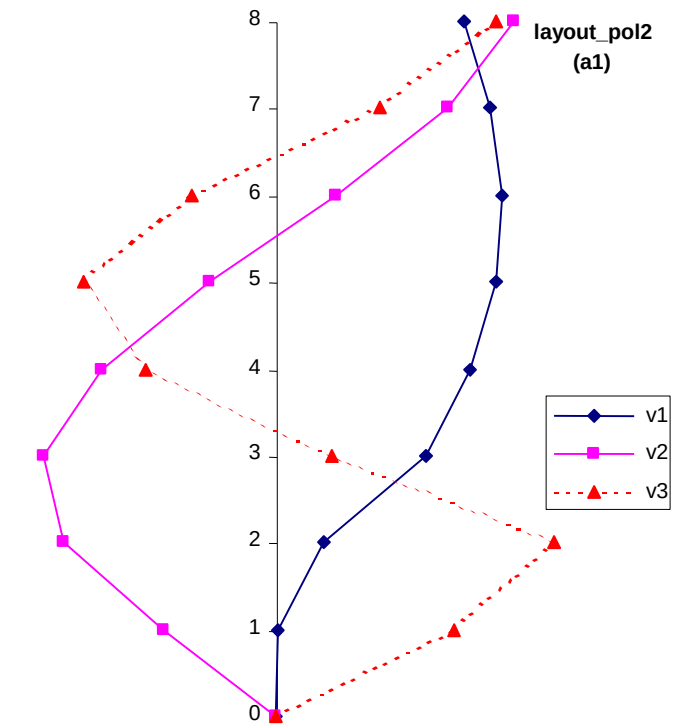

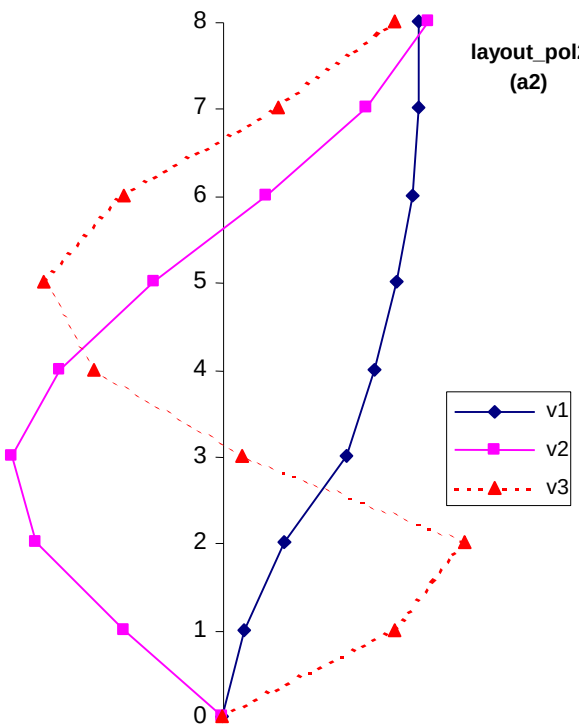

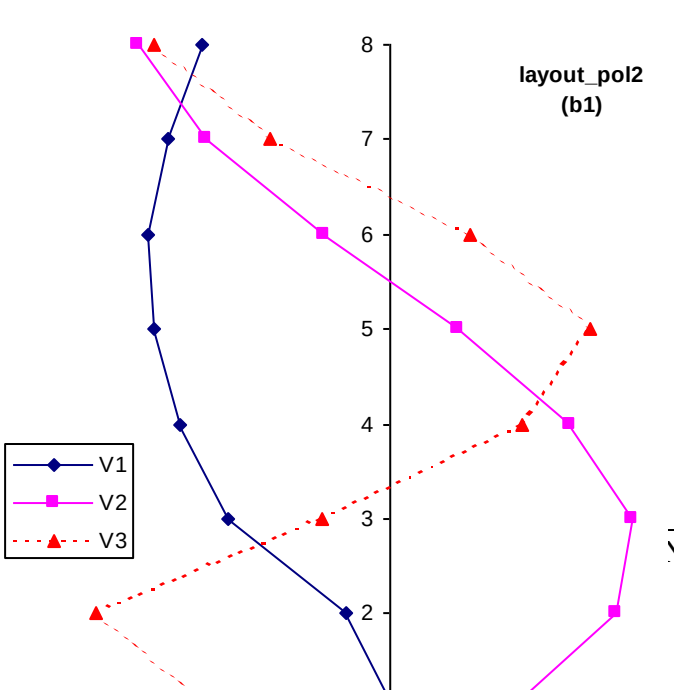

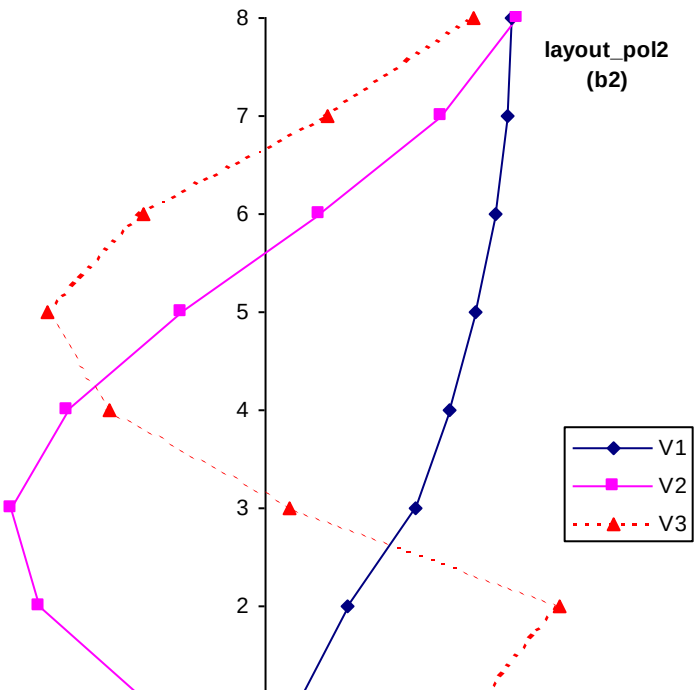

Fig. 3.1.9. Pol2 layout: eigenvectors.

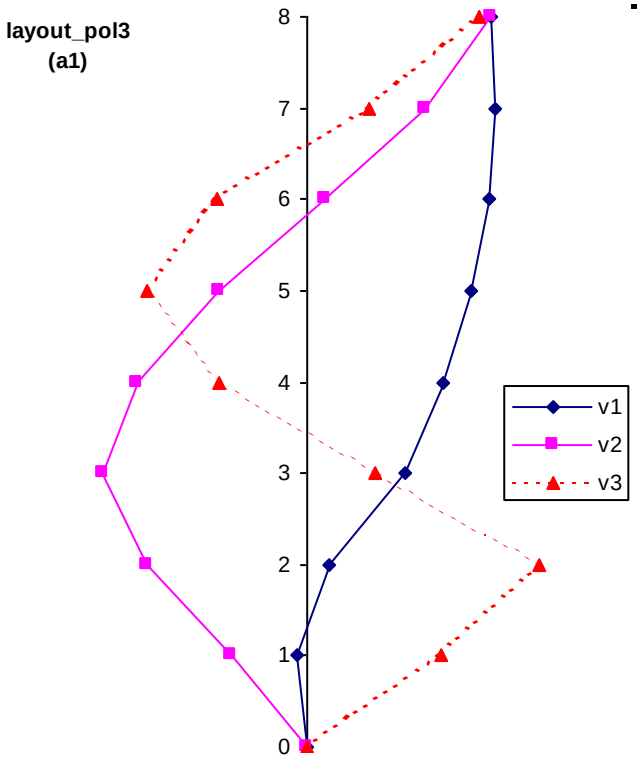

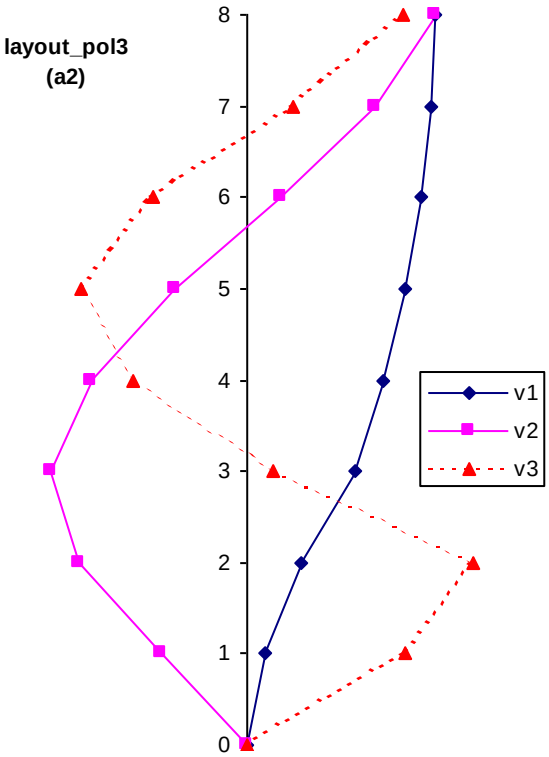

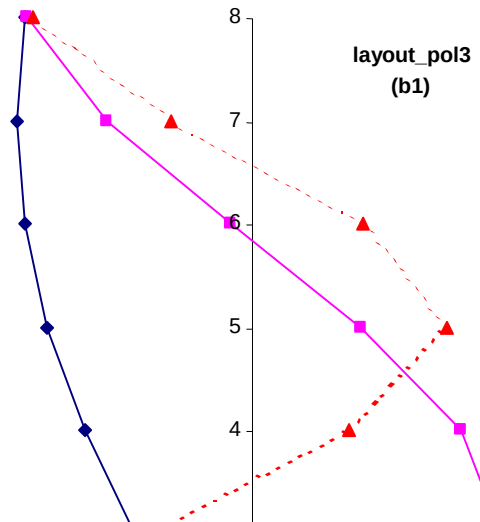

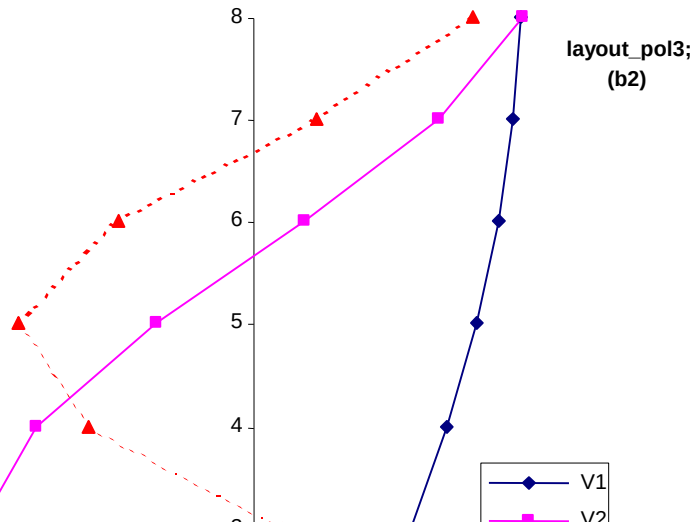

Fig. 3.1.10. Pol3 layout: eigenvectors.

4-storey building

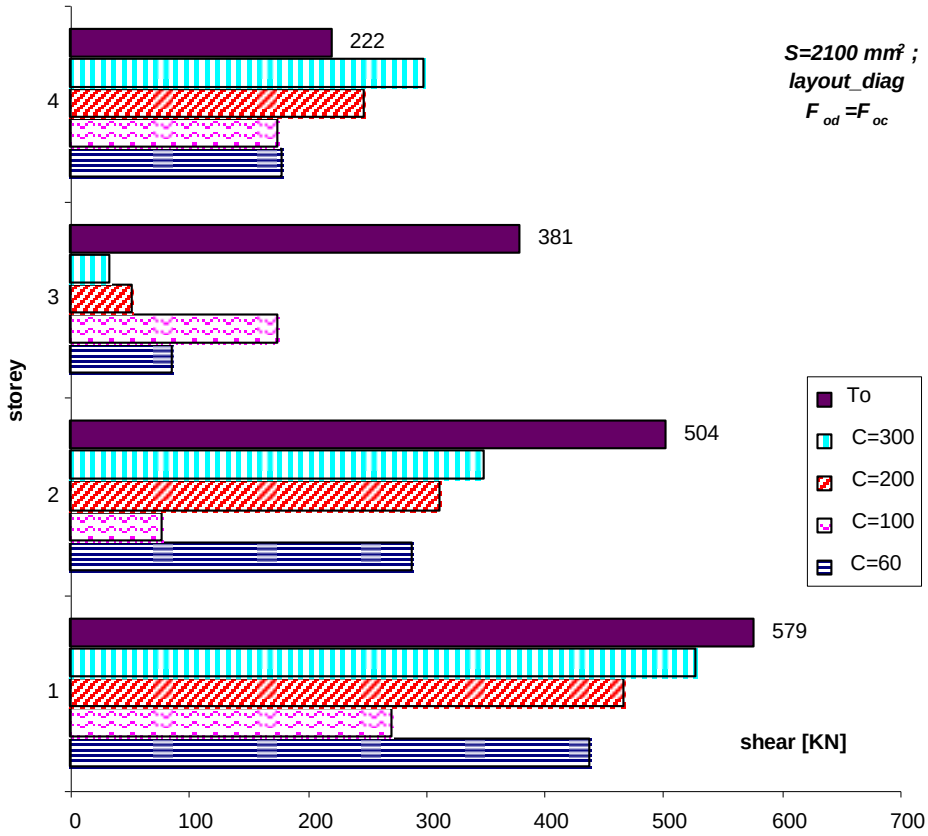

Fig. 3.2.1. Diagonal layout: storey shear as a function of C.

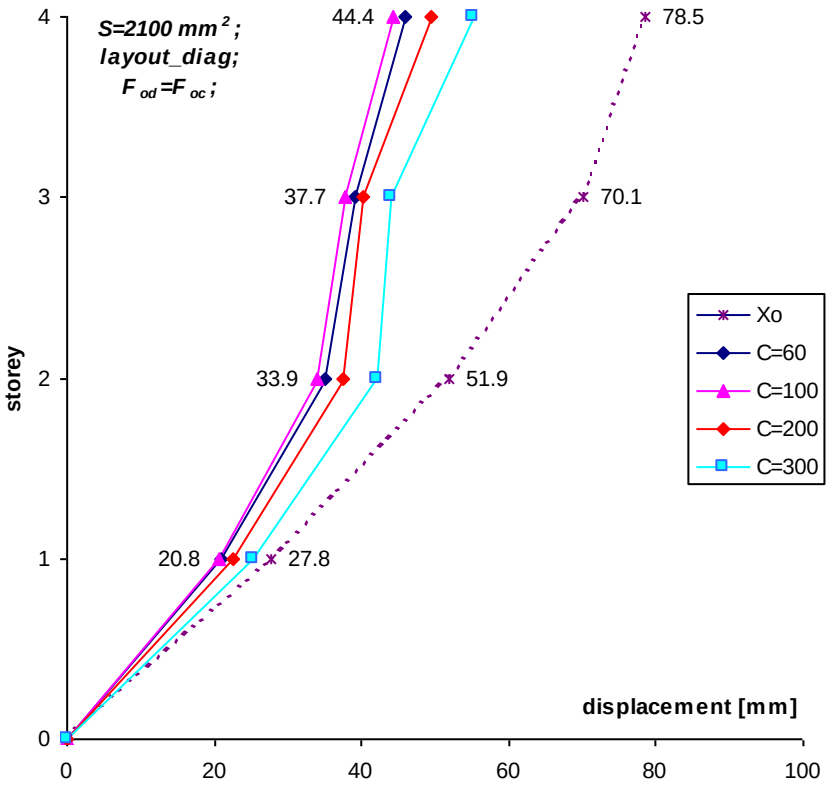

Fig. 3.2.2. Diagonal layout: storey displacement as a function of C.

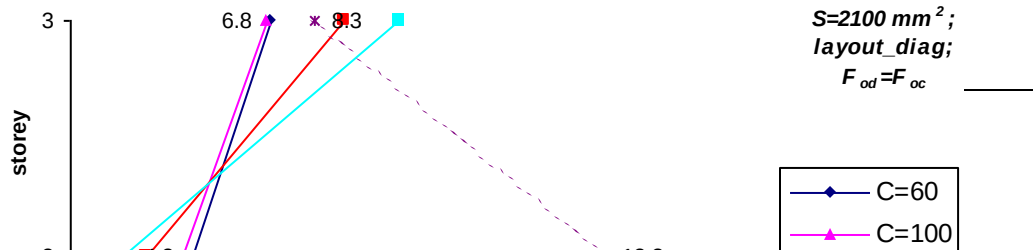

Fig. 3.2.3. Diagonal layout: interstorey drifts.

8-storey building

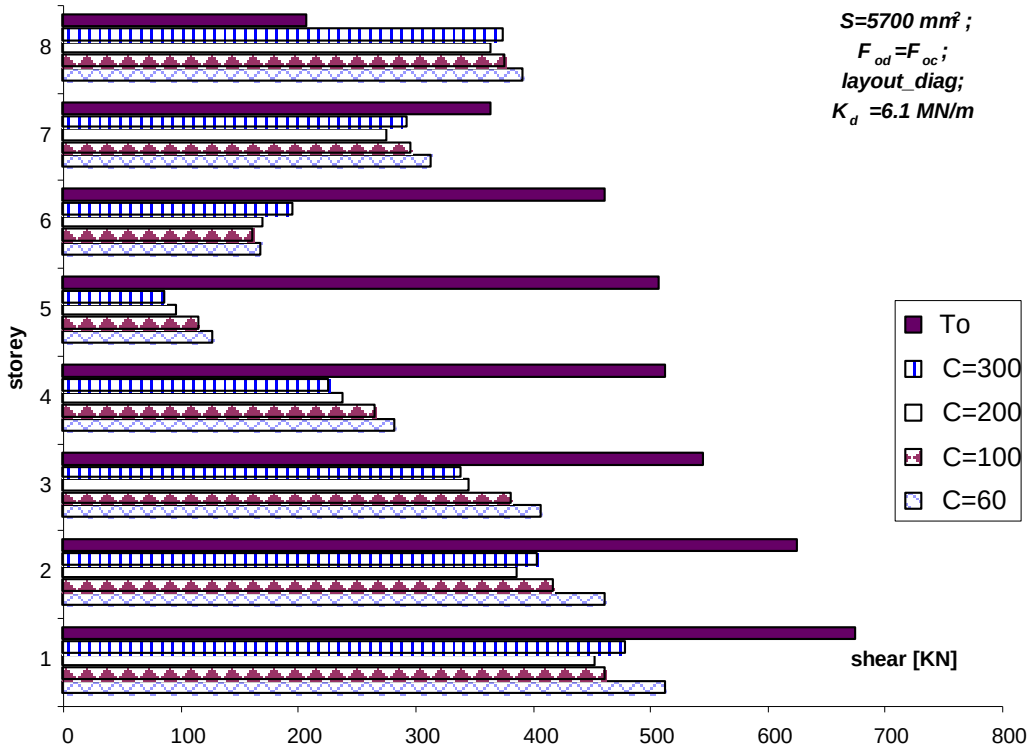

Fig. 3.2.4. Diagonal layout: storey shear as a function of C.

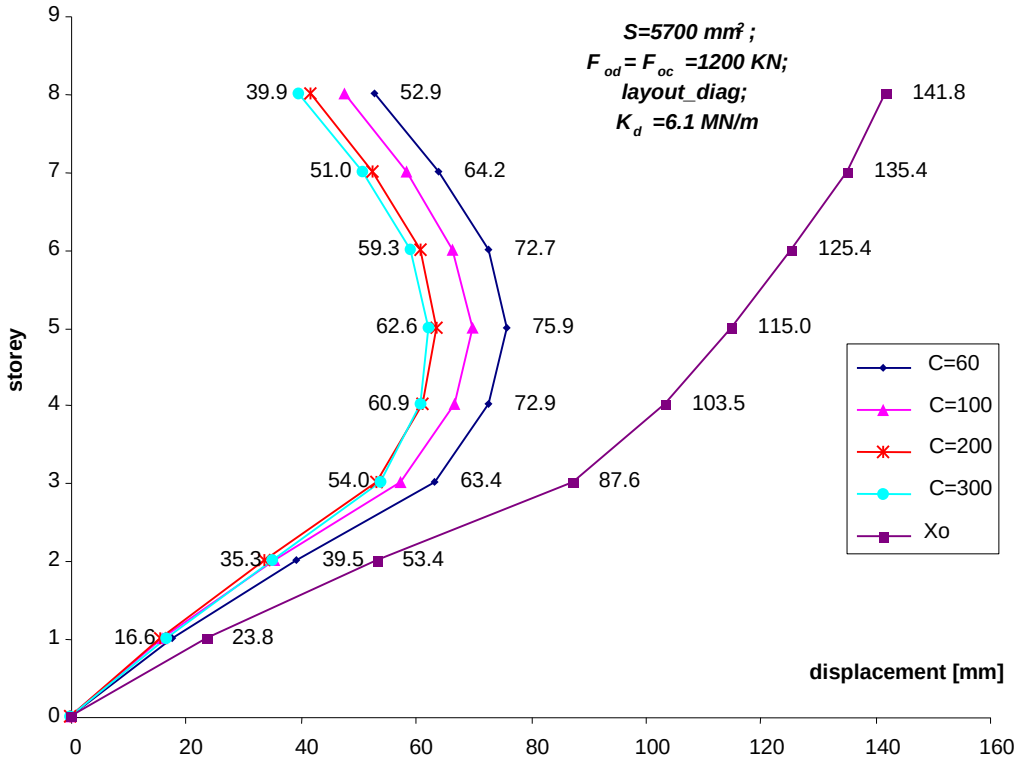

Fig. 3.2.5. Diagonal layout: storey displacement as a function of C.

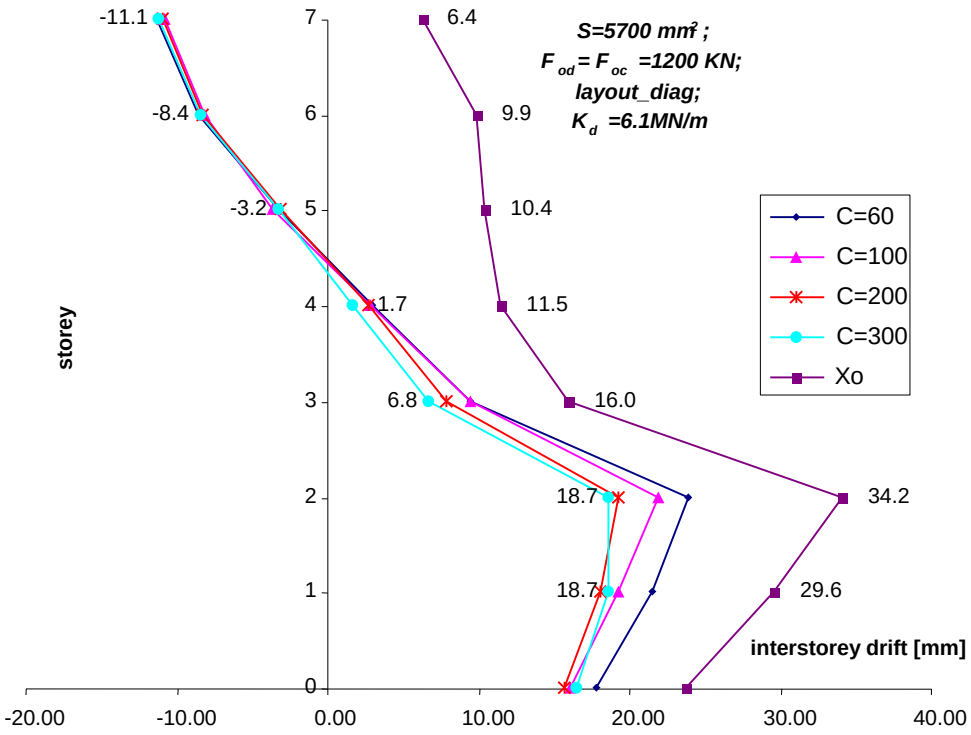

Fig. 3.2.6. Diagonal layout: interstorey drifts as a function of C.

10-storey building

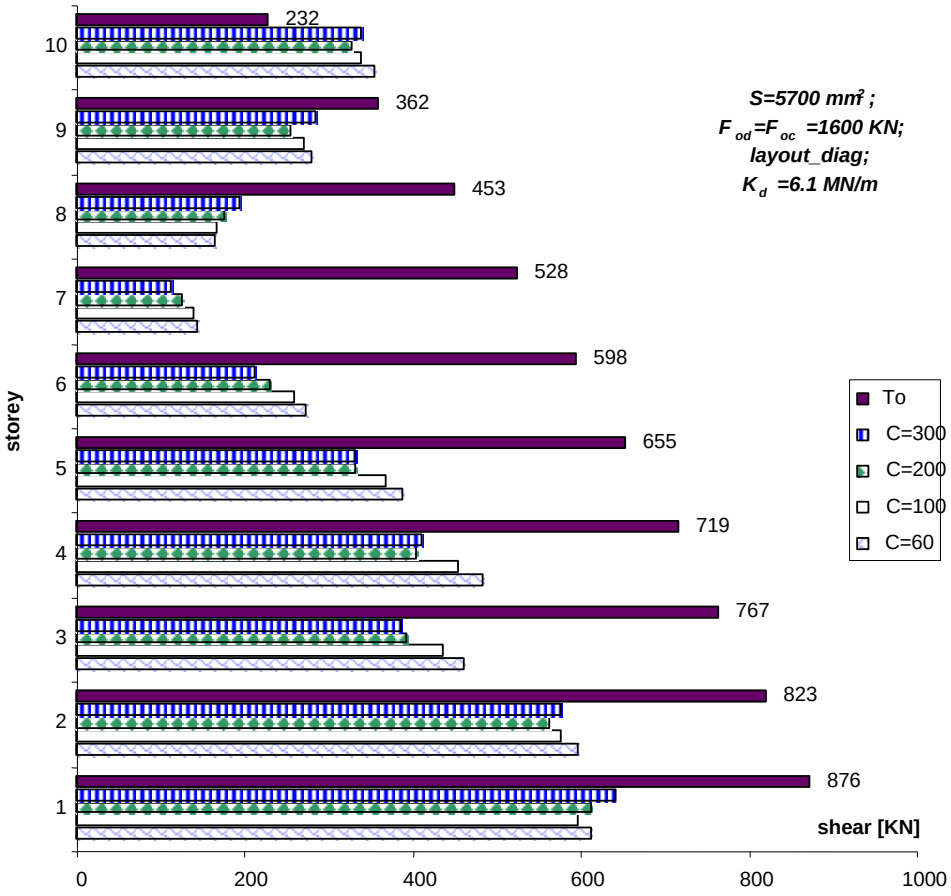

Fig. 3.2.7. Diagonal layout: storey shear as a function of C.

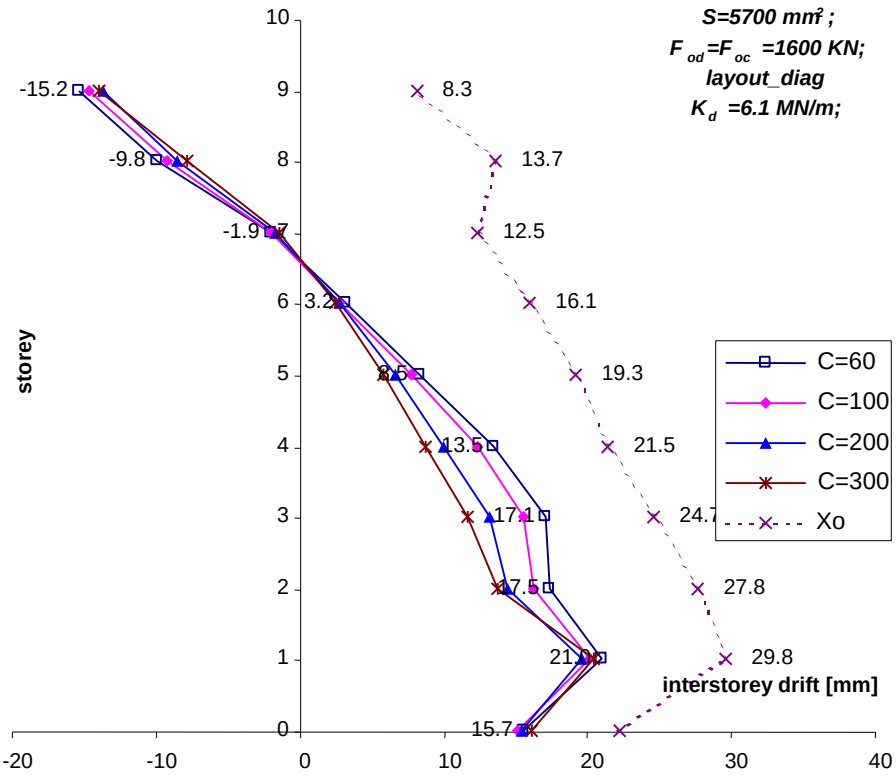

Fig. 3.2.8. Diagonal layout: interstorey drift as a function of C.

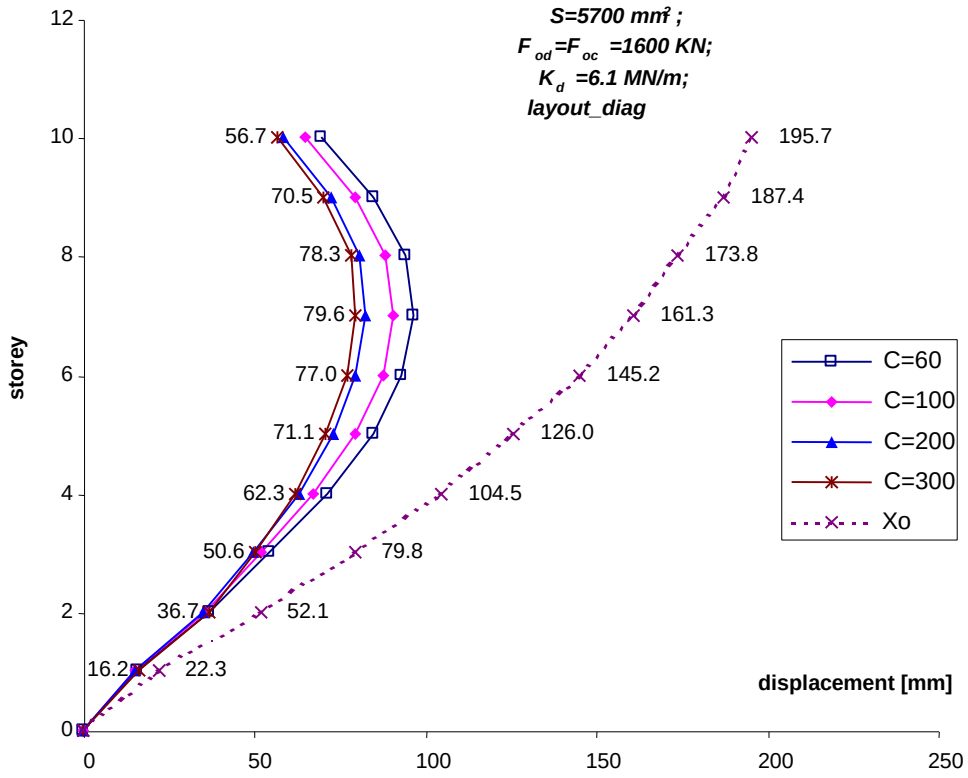

Fig. 3.2.9. Diagonal layout: storey displacement as a function of C.

4-storey building

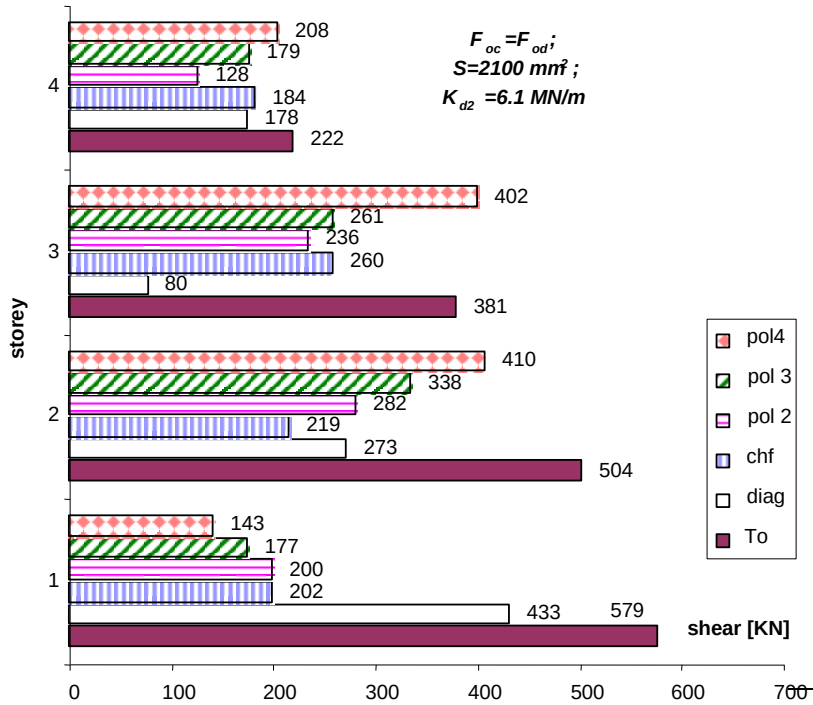

Fig. 3.2.10. Story shear as a function of cable layout. For each layout the selected C value is the one minimising story shear.

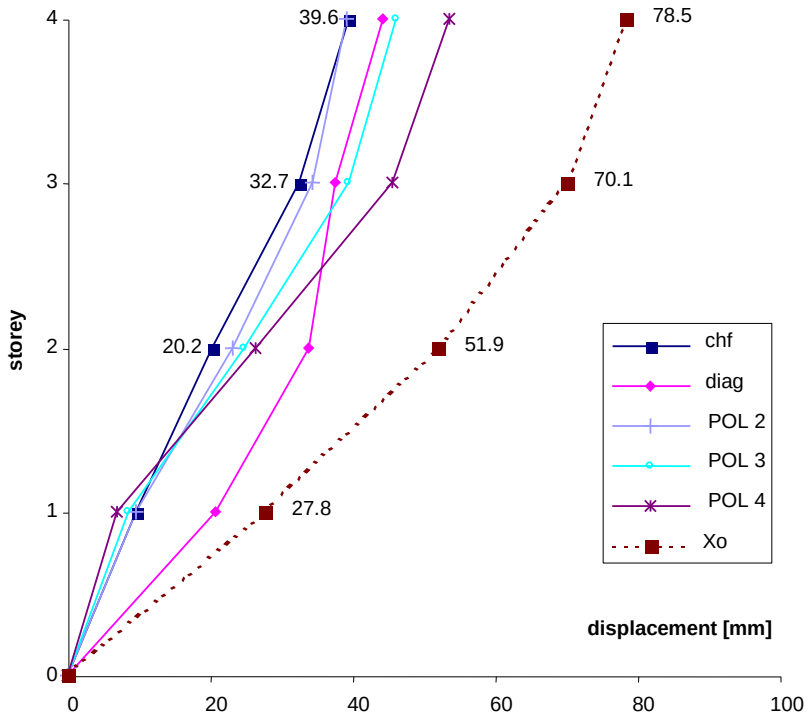

Fig. 3.2.11. Interstorey drift as a function of cable layout.

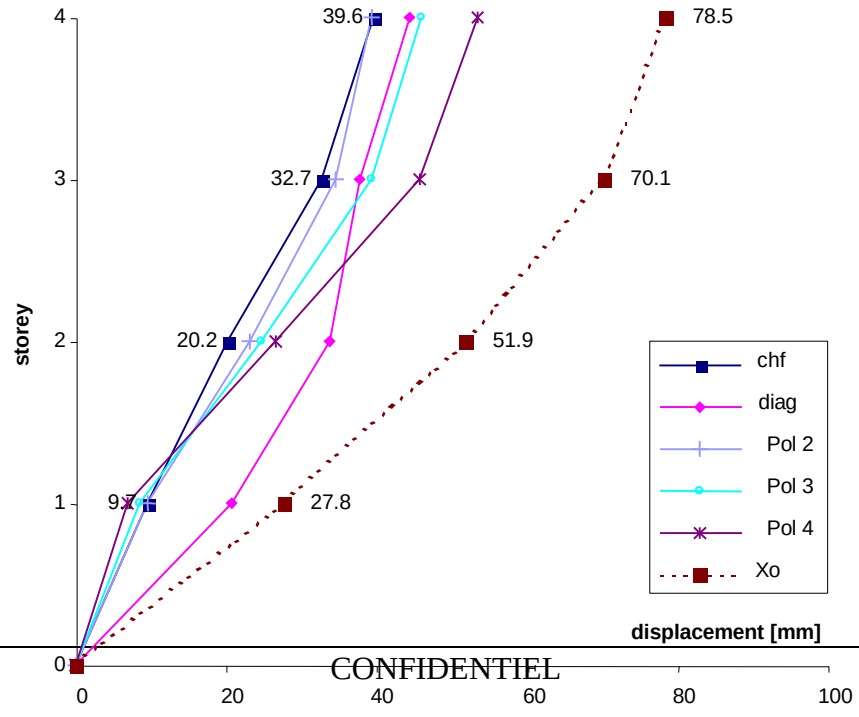

Fig. 3.2.12. Storey displacement as a function of cable layout.

8–storey building

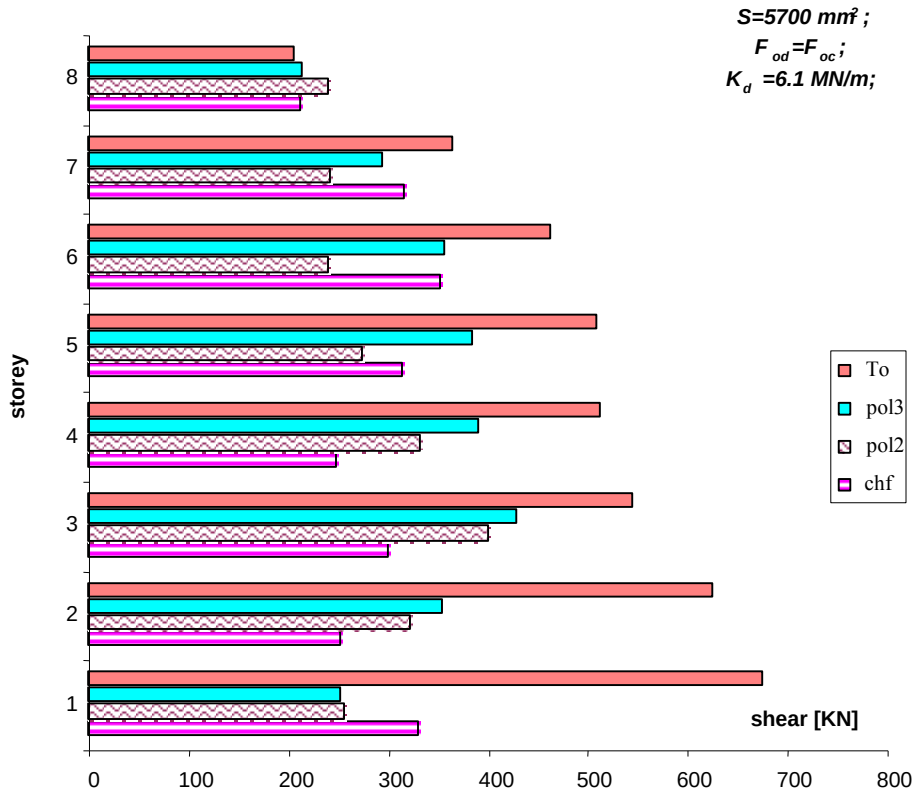

Fig. 3.2.13. Storey shear as a function of cable layout.

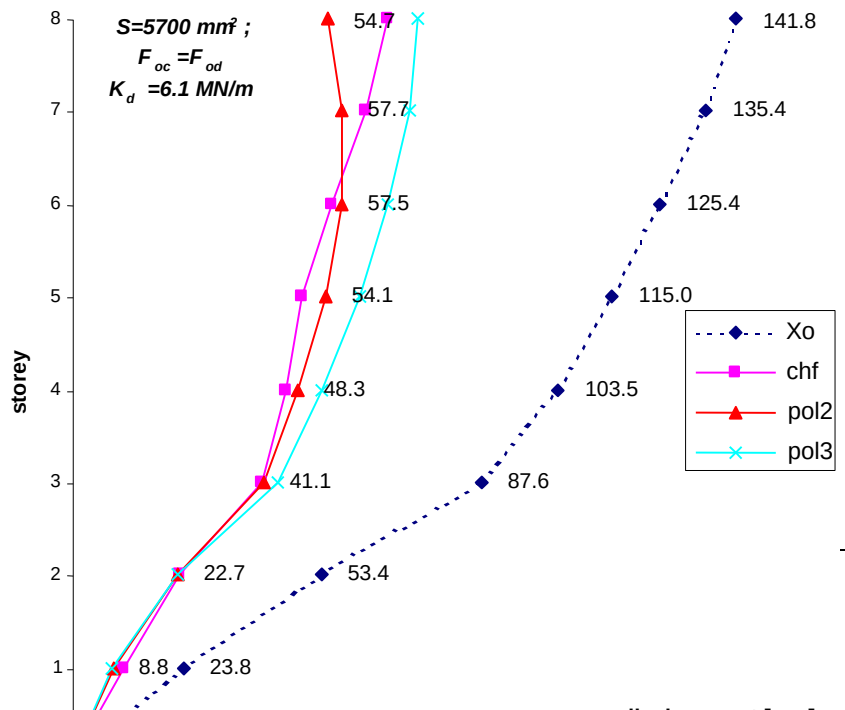

Fig. 3.2.14. Storey displacement as a function of cable layout.

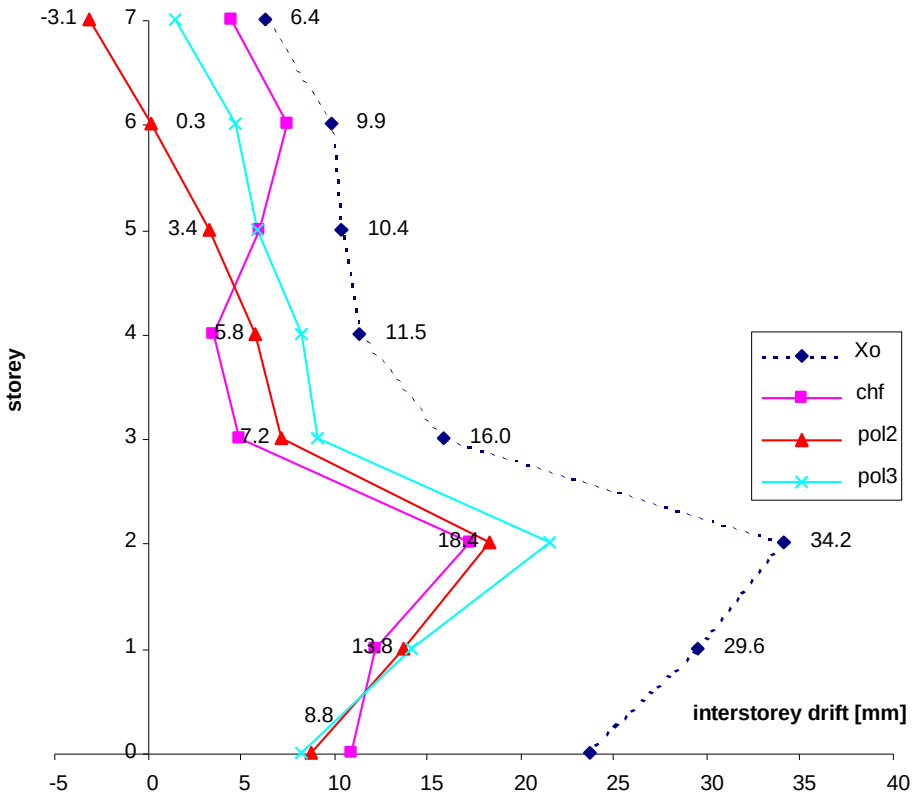

Fig. 3.2.15. Interstorey drift as a function of cable layout.

10-storeys building

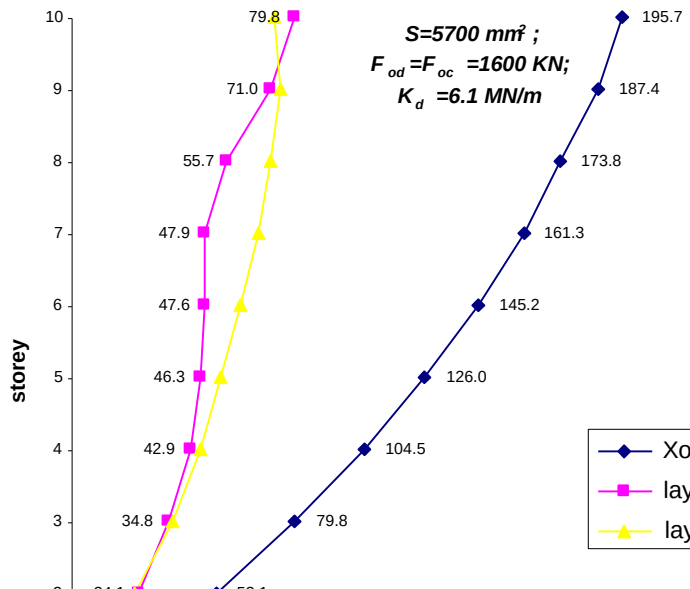

Fig. 3.2.16. Storey displacement as a function of cable layout.

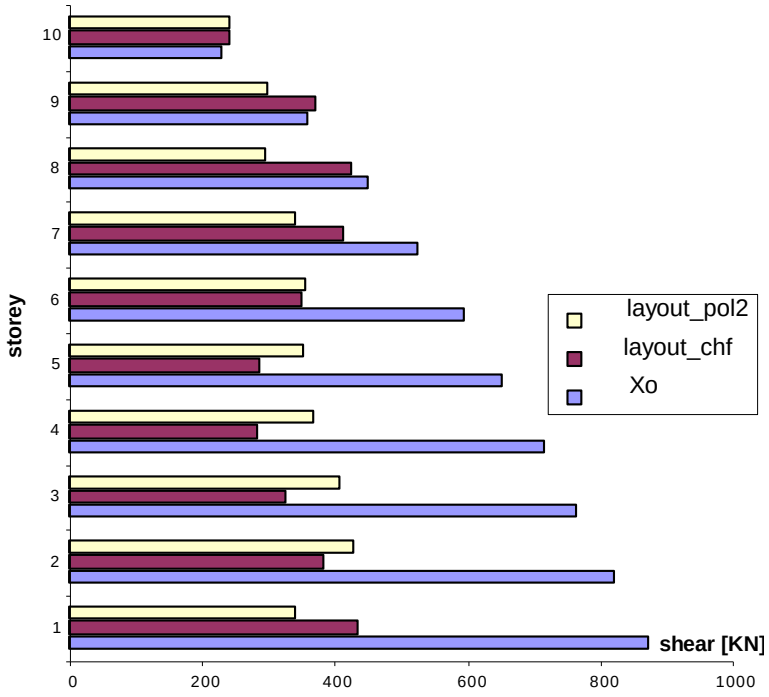

Fig. 3.2.17. Story shear as a function of cable layout.

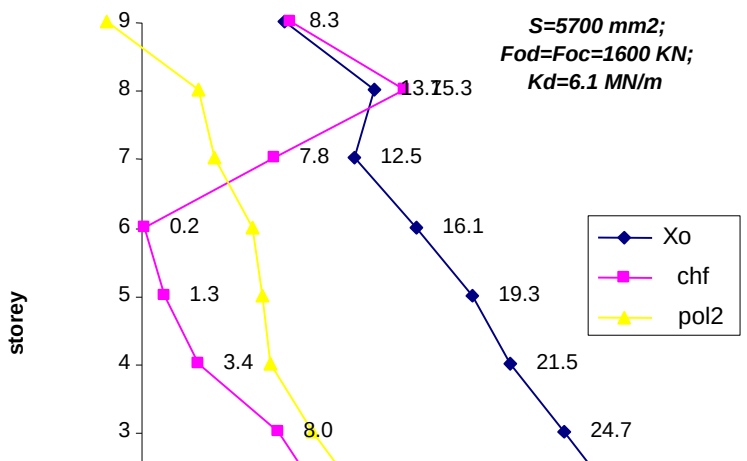

Fig. 3.2.18. Interstorey drifts as a function of cable layout.

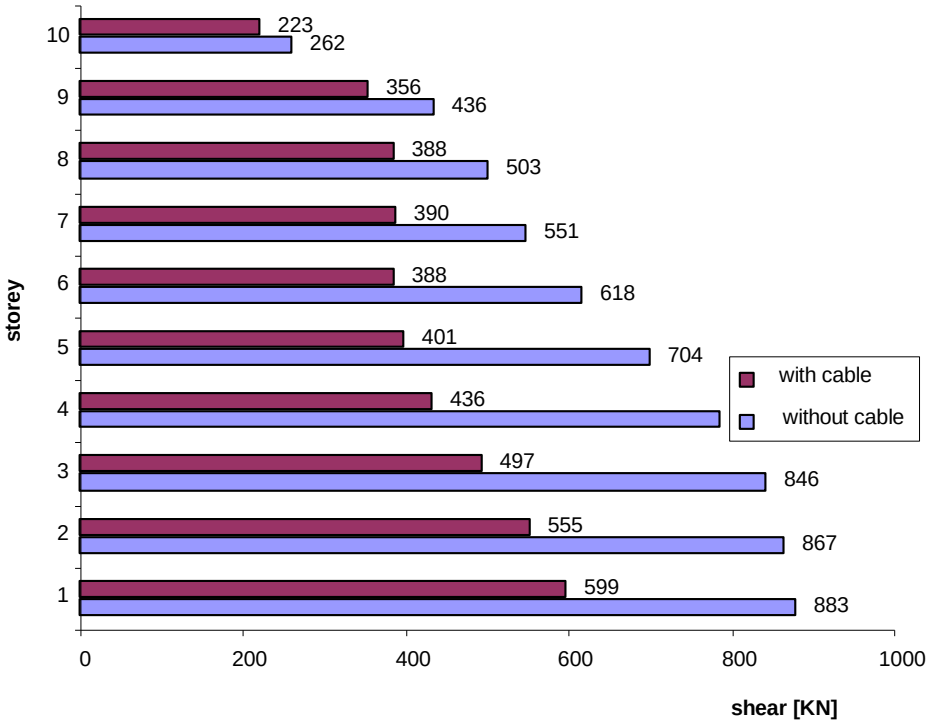

Fig. 3.2.19. Storey shear. CHF layout; $F_{od}=F_{oc}=K_c\Delta l_{oc}/2$; $K_d=6.1$ MN/m; $S_c=5700$ mm^2.

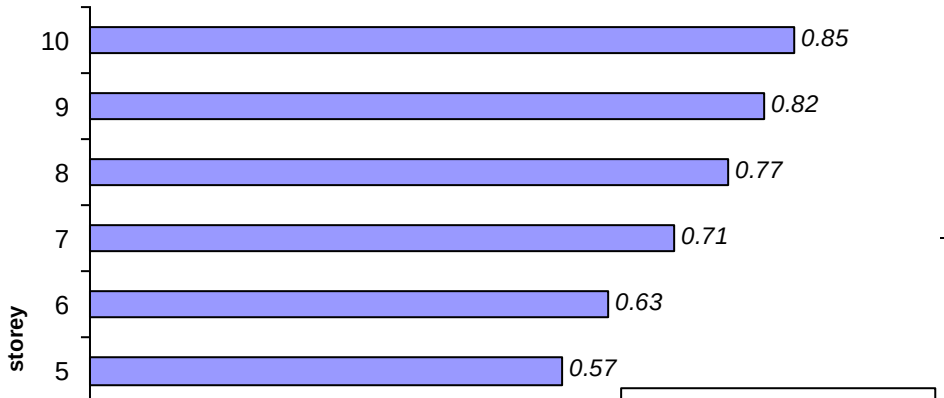

Fig. 3.2.20. Ratio between storey shear for structure with and without cable.

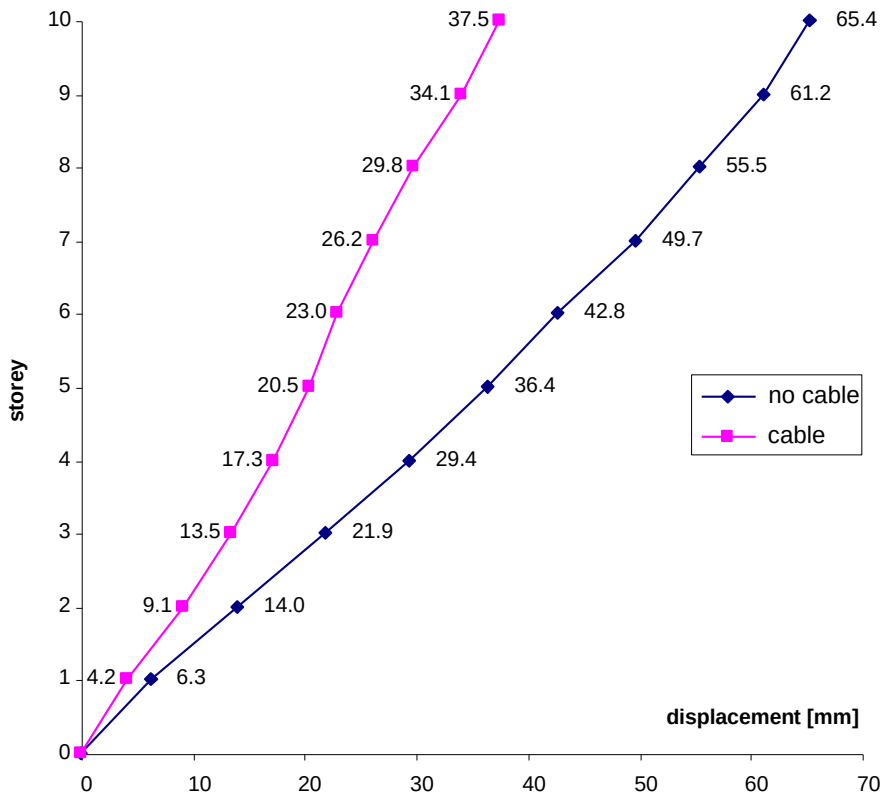

Fig. 3.2.21. Storey displacement for structure with and without cable.

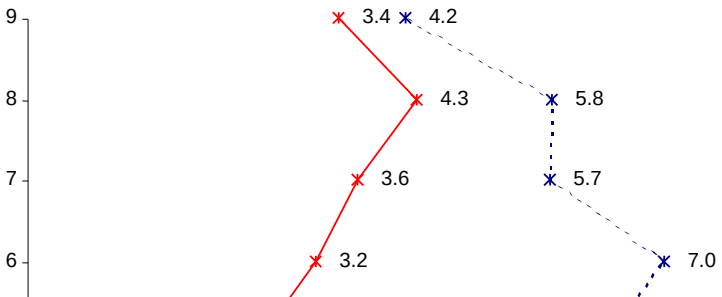

Fig. 3.2.22. Interstorey drift for structure with and without cable.

EC8 dual structure

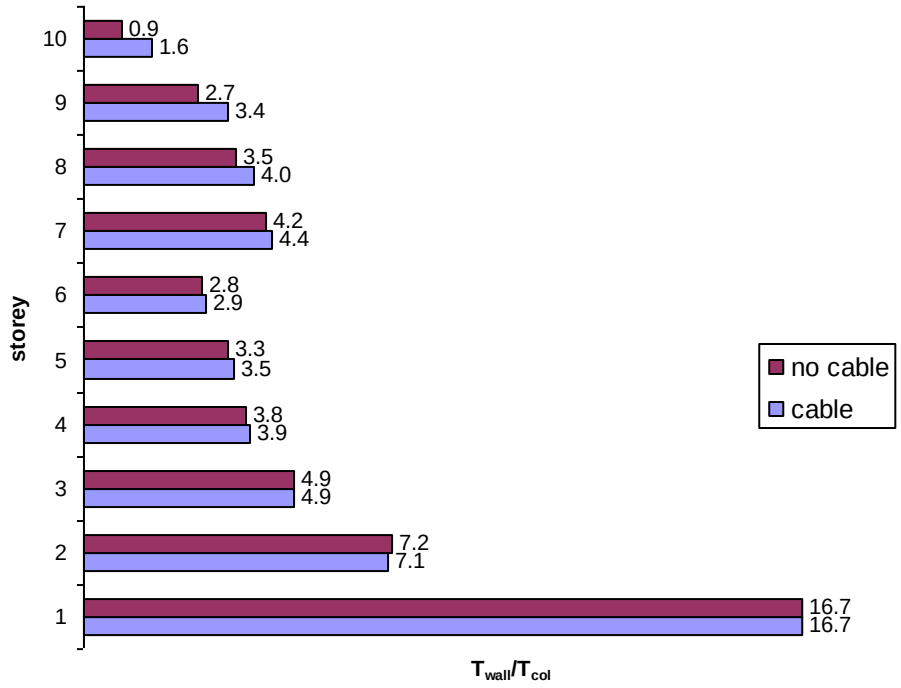

Fig. 3.2.23. Wall/frame storey shear ratio for structure with and without cable. CHF layout; S_c=5700 mm^2; $F_{od}=F_{oc}=K_c\Delta l_{oc}/2$; K_d=6.1 MN/m.

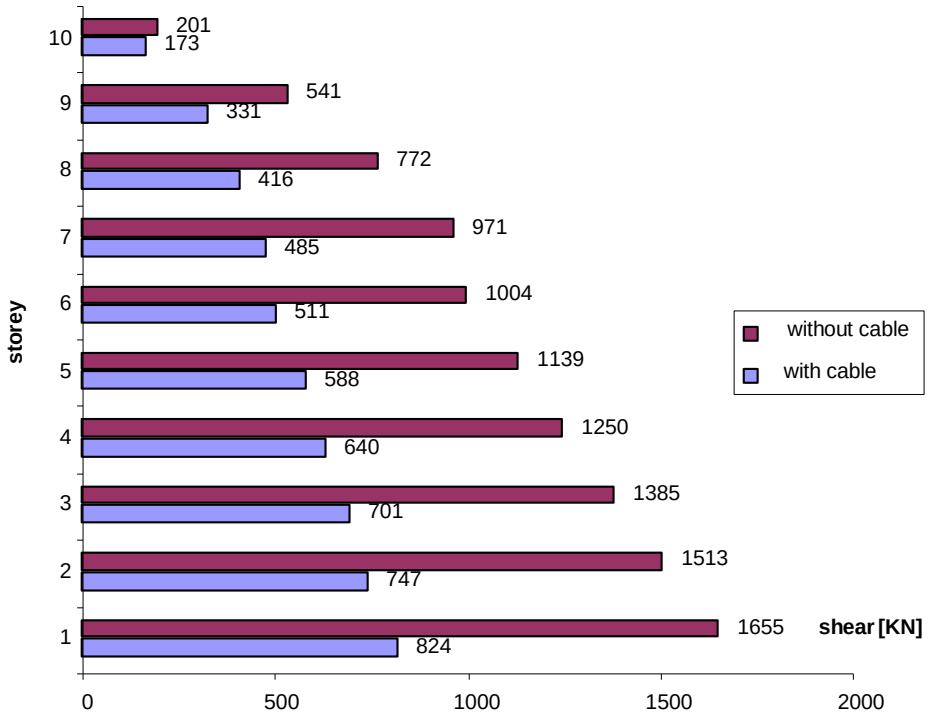

Fig. 3.2.24. Wall storey shear for structure with and without cable.

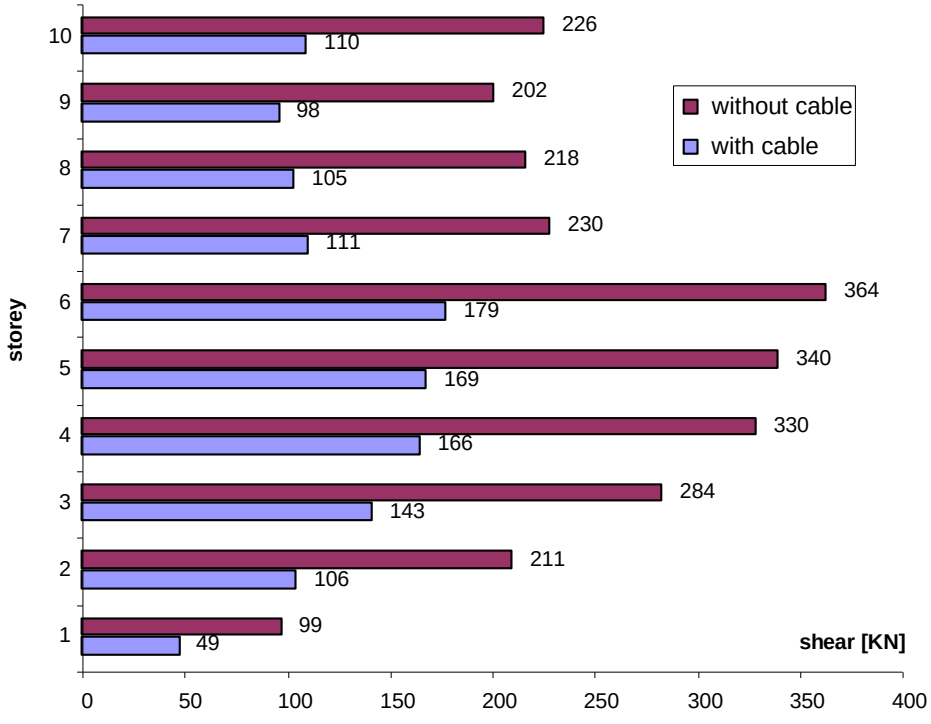

Fig. 3.2.25. Frame storey shear for structure with and without cable.

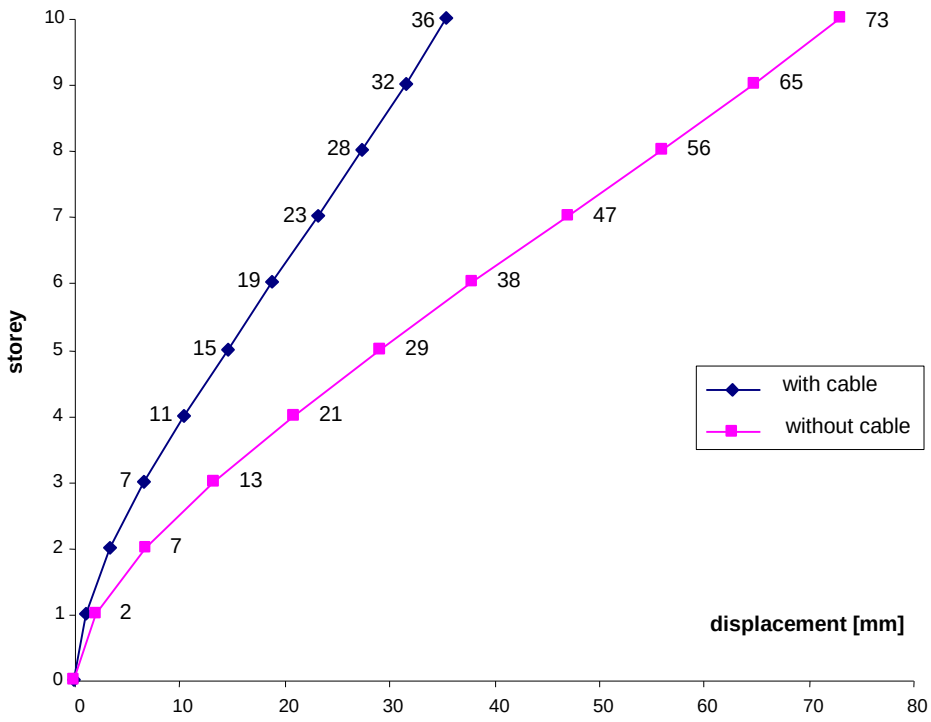

Fig. 3.2.26. Storey displacements for structure with and without cable.

4-storey building

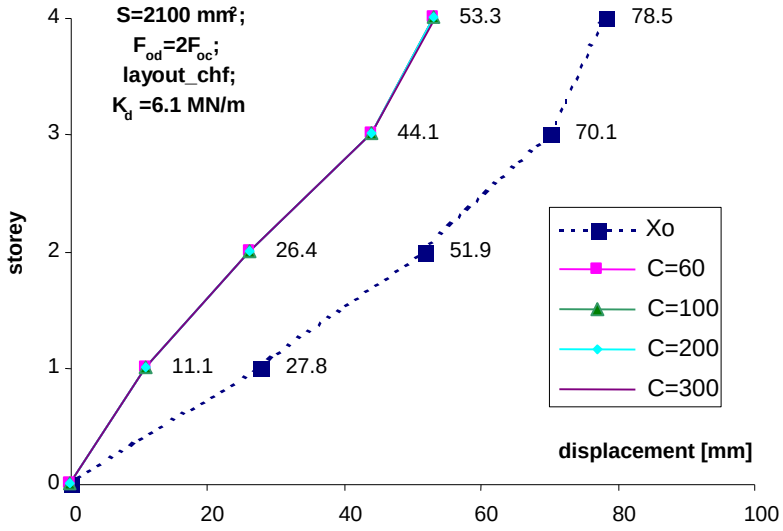

Fig. 3.3.1. Storey displacement as a function of C.

CHF layout; S_c=2100 mm^2; F_{od}=2F_{oc}=$K_c\Delta l_{oc}$; K_d=6.1 MN/m.

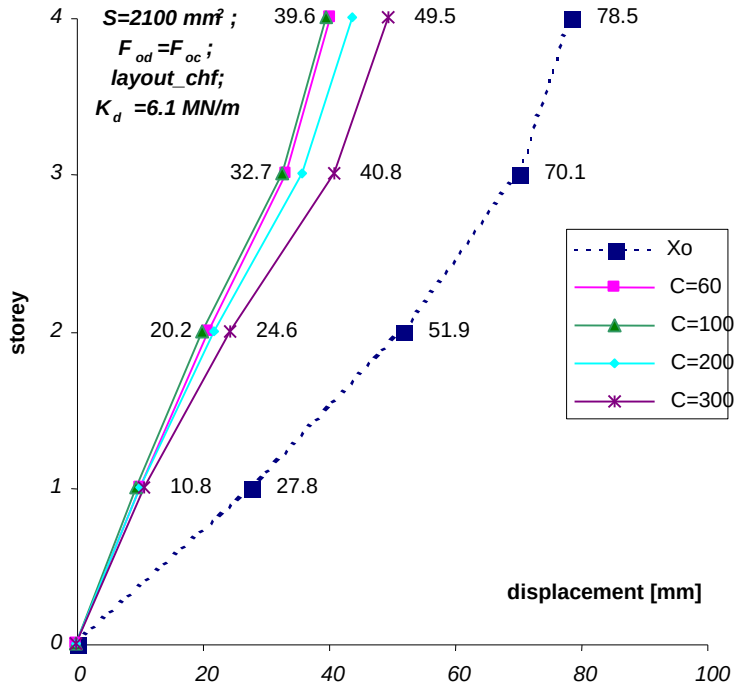

Fig. 3.3.2. Storey displacement as a function of C.

CHF layout; S_c=2100 mm^2; F_{od}=F_{oc}=$K_c\Delta l_{oc}$/2; K_d=6.1 MN/m.

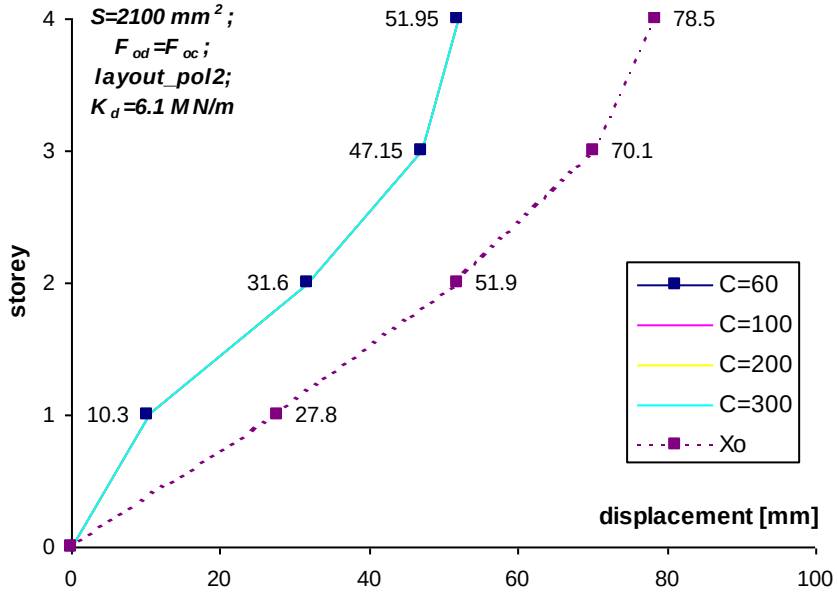

Fig. 3.3.3. Storey displacement as a function of C.

Pol2 layout; S_c=2100 mm^2; $F_{od}=2F_{oc}=K_c\Delta l_{oc}$; K_d=6.1 MN/m.

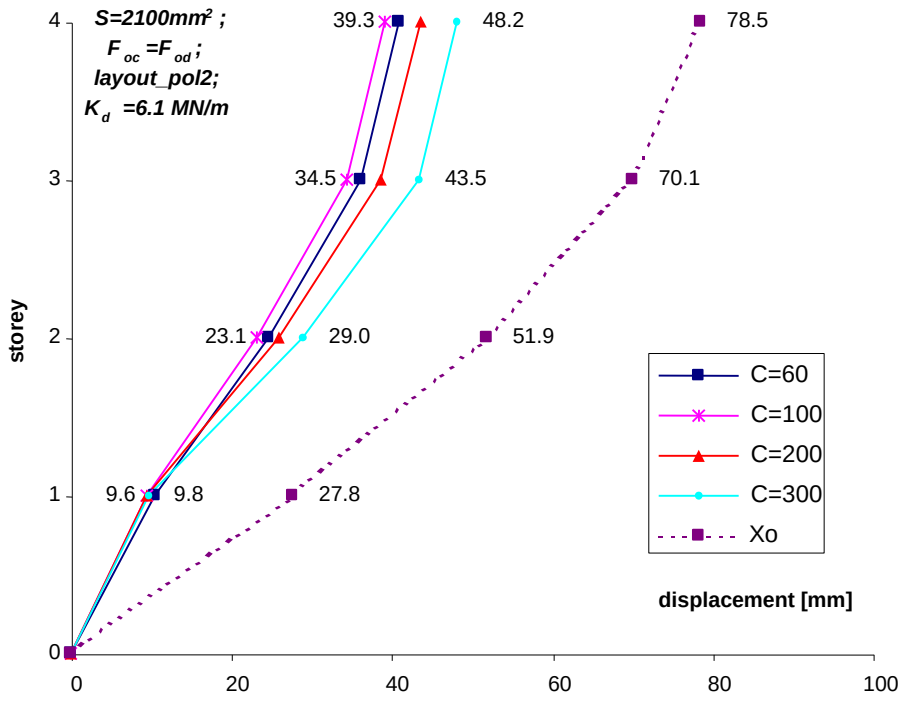

Fig. 3.3.4. Storey displacement as a function of C.

Pol2 layout; S_c=2100 mm^2; $F_{od}=F_{oc}=K_c\Delta l_{oc}/2$; K_d=6.1 MN/m.

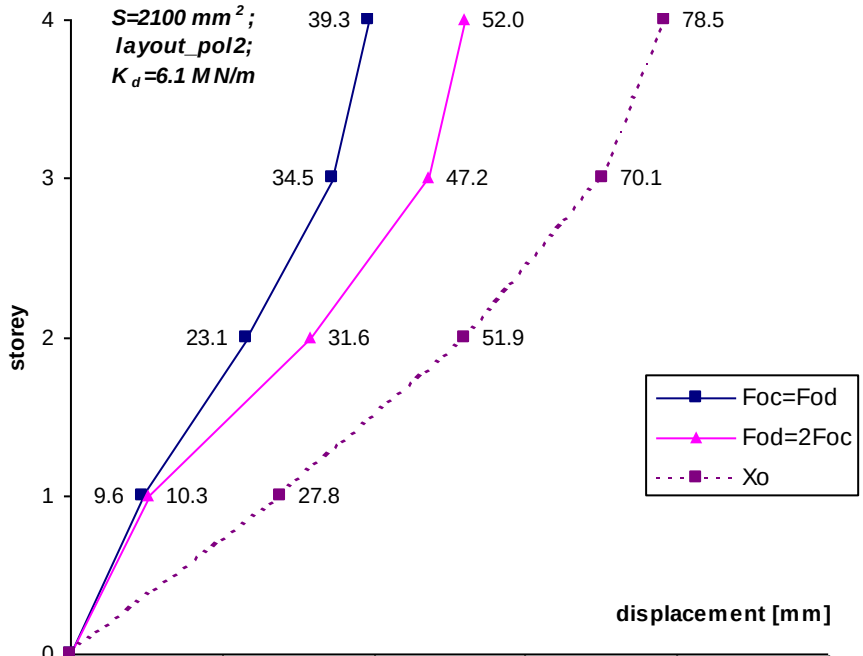

Fig. 3.3.5. Comparison between storey displacements obtained for $F_{od}=F_{oc}$ and $F_{od}=2F_{oc}$.

Pol2 layout; $S_c=2100\ mm^2$; $C=60\ kN(s/m)^{\alpha}$; $K_d=6.1\ MN/m$.

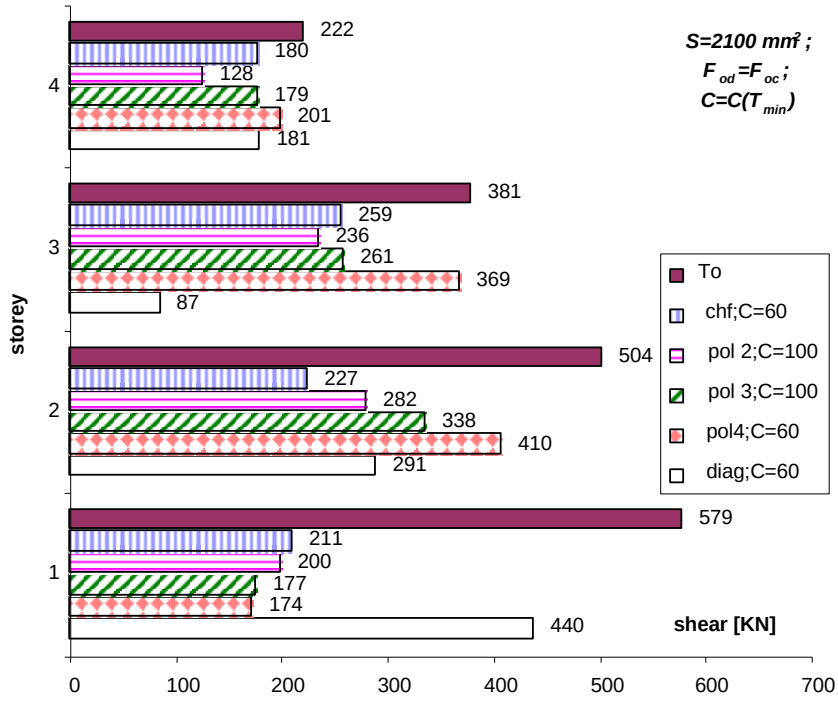

Fig. 3.3.6. Storey shear as a function of cable layout.

$S_c=2100\ mm^2$; $F_{od}=2F_{oc}=K_c\Delta l_{oc}$; $K_d=6.1\ MN/m$ (for each layout C is equal to the value that minimises shear).

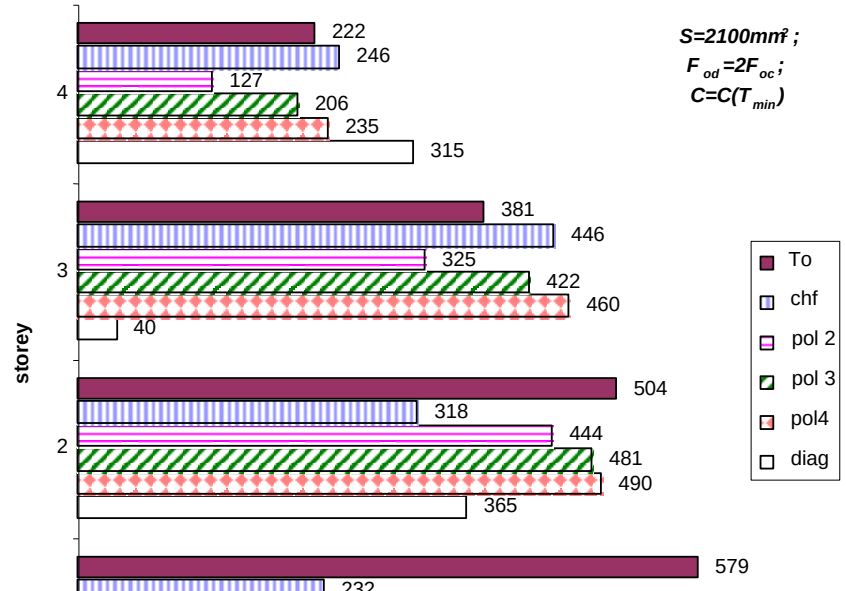

Fig. 3.3.7. Storey shear as a function of cable layout. S_c=2100 mm^2; $F_{od}=F_{oc}=K_c\Delta l_{oc}/2$; K_d=6.1 MN/m (for each layout C is equal to the value that minimises shear)

4-storey building

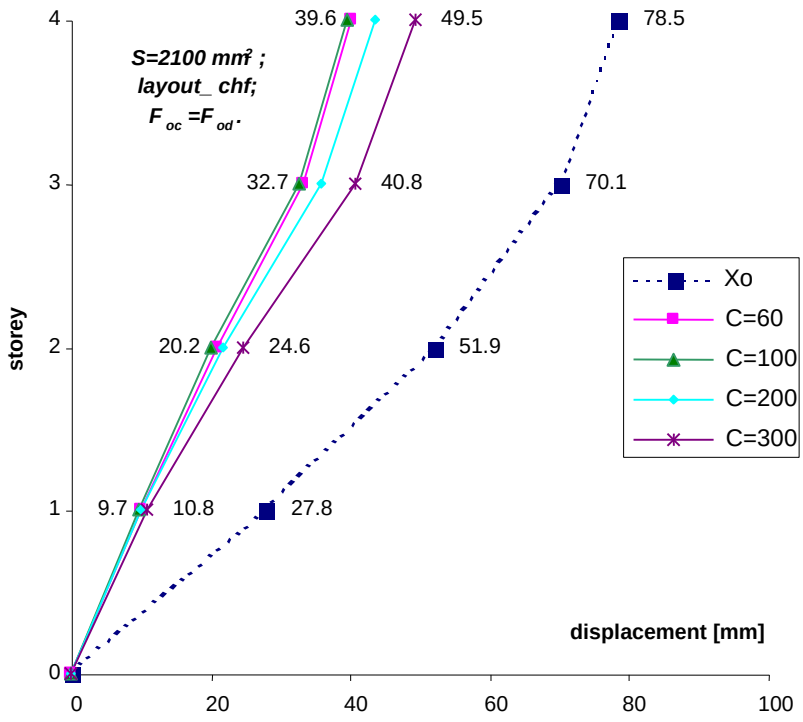

Fig. 3.4.1. Storey displacement as a function of C

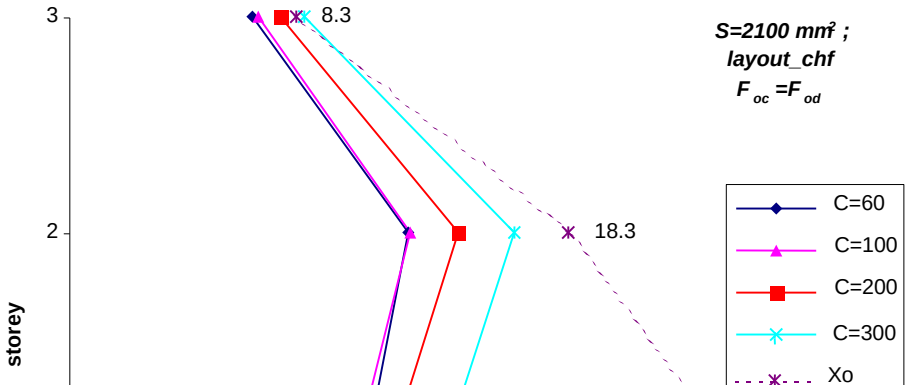

Fig. 3.4.2. Interstorey drift as a function of C.

S_c=2100 mm^2; $F_{od}=F_{oc}=K_c\Delta l_{oc}/2$; K_d=6.1 MN/m.

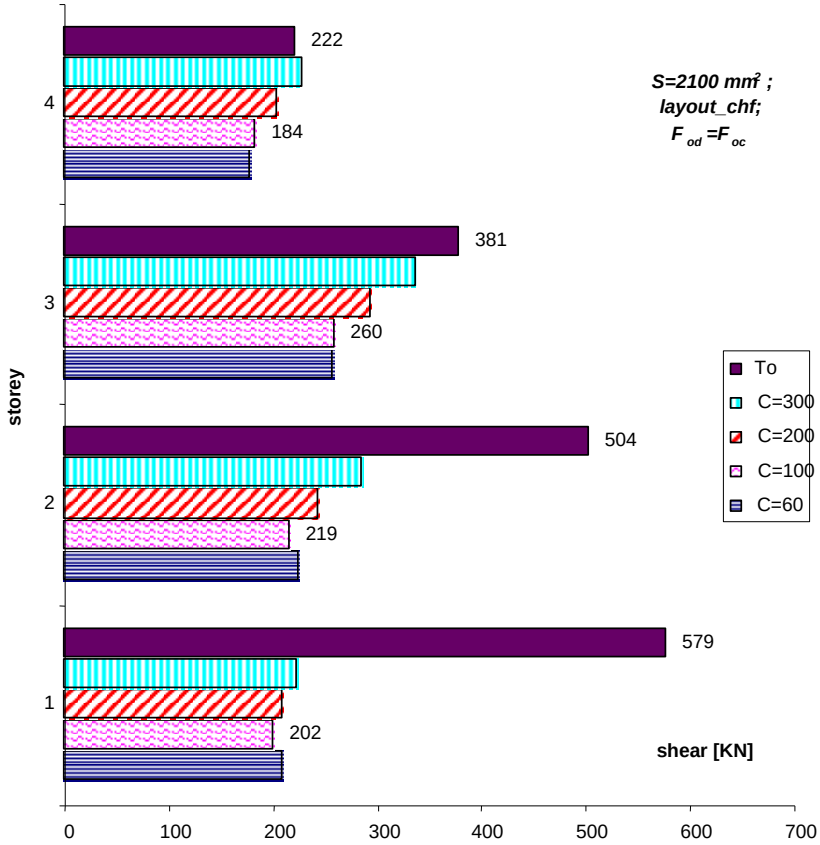

Fig. 3.4.3. Storey shear as a function of C.

S_c=1050 mm^2; $F_{od}=F_{oc}=K_c\Delta l_{oc}/2$; K_d=6.1 MN/m.

8-storey building

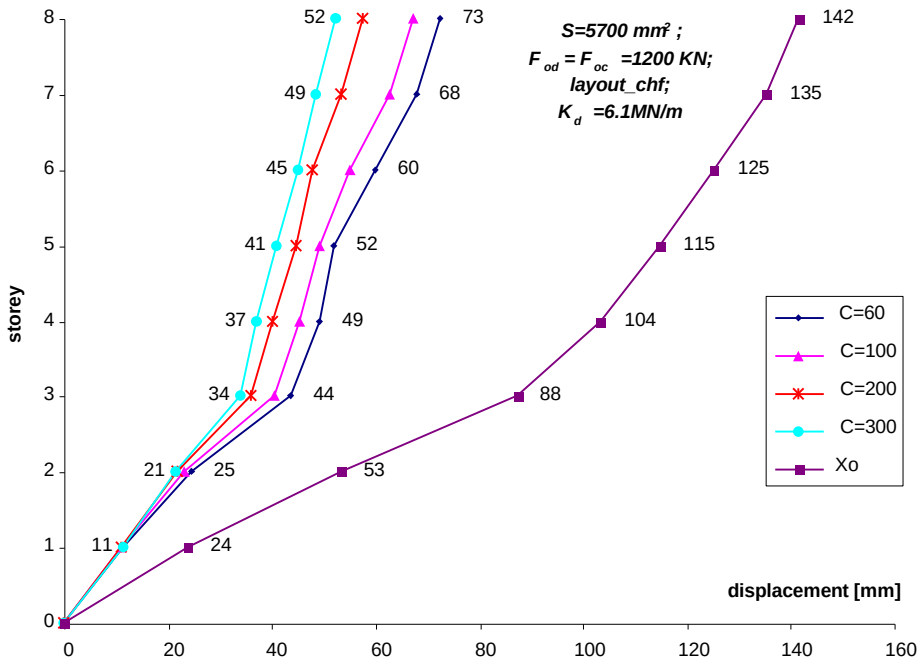

Fig. 3.4.4. Storey displacement as a function of C.

S_c=5700 mm^2; $F_{od}=F_{oc}=K_c\Delta l_{oc}/2$; K_d=6.1 MN/m.

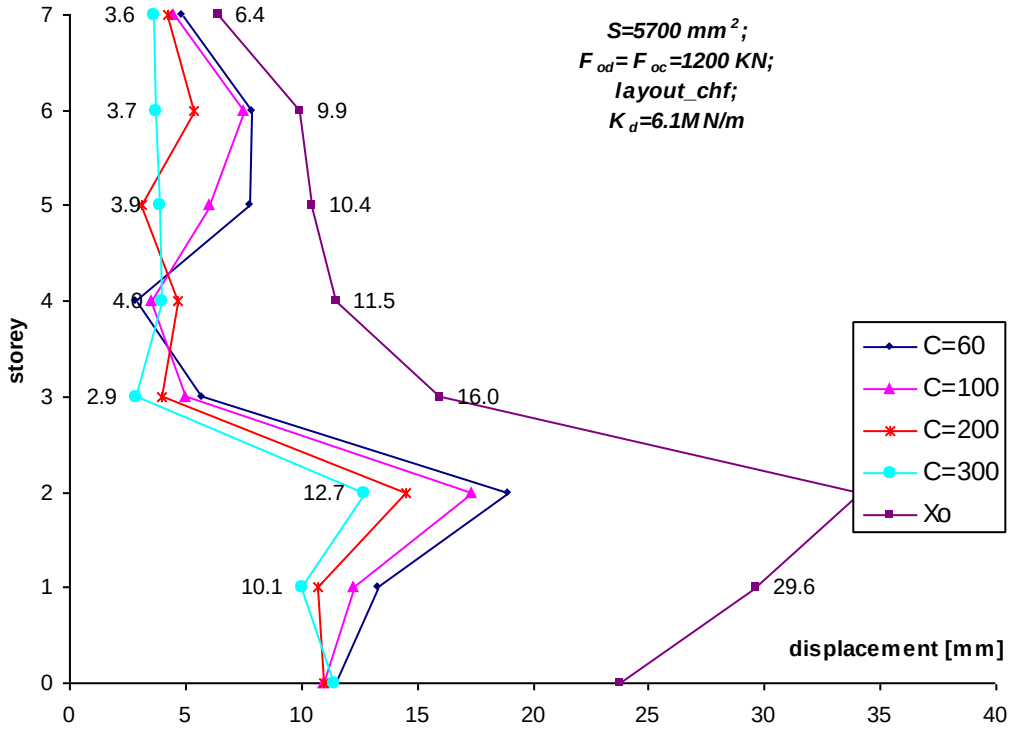

Fig. 3.4.5. Interstorey drift as a function of C.

S_c=5700 mm^2; $F_{od}=F_{oc}=K_c\Delta l_{oc}/2$; K_d=6.1 MN/m.

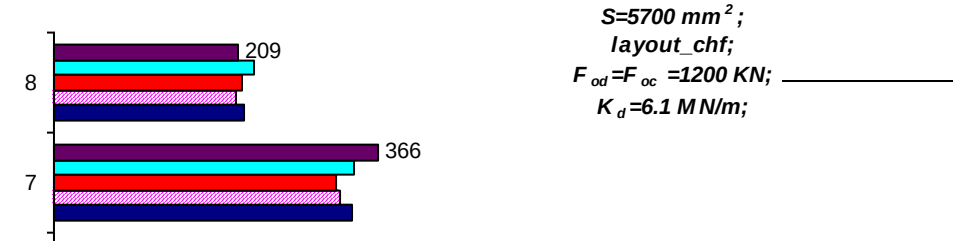

Fig. 3.4.6. Storey shear as a function of C.

$S_c=5700\ mm^2$; $F_{od}=F_{oc}=K_c\Delta l_{oc}/2$; $K_d=6.1\ MN/m$.

8-storey building

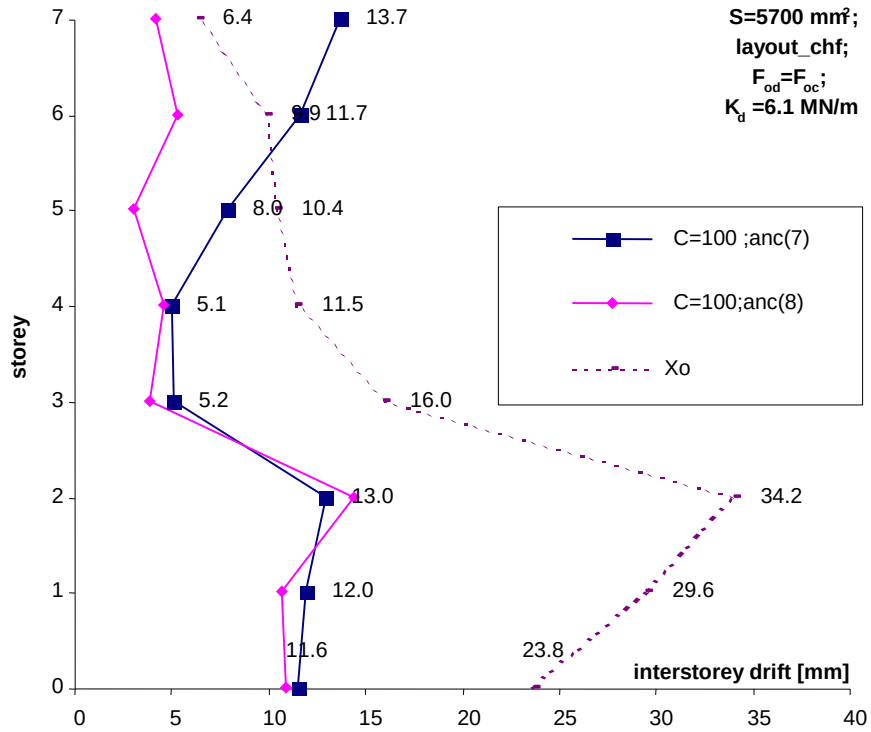

Fig. 3.5.1. Interstorey drifts obtained for upper anchorage level at 8-th or 7-th floors.

CHF layout; S_c=5700 mm^2; $F_{od}=F_{oc}=K_c\Delta l_{oc}/2$; C=100 kN(s/m)$^{\alpha}$; K_d=6.1 MN/m.

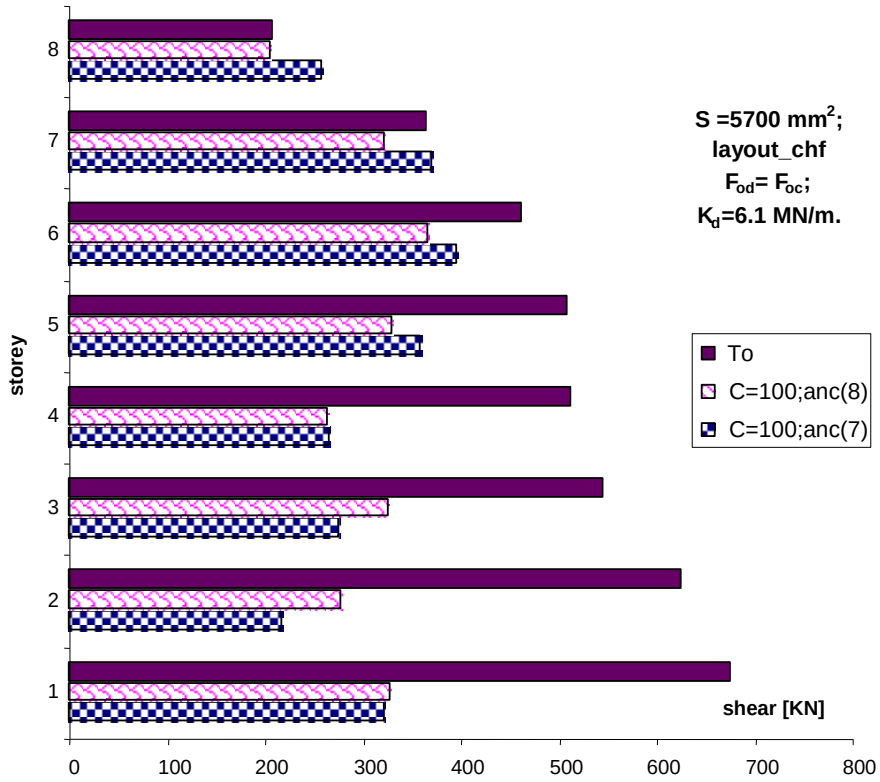

Fig. 3.5.2. Storey shears obtained for upper anchorage level at 8-th or 7-th floors.

CHF layout; S_c=5700 mm^2; $F_{od}=F_{oc}=K_c\Delta l_{oc}/2$; C=100 kN(s/m)$^{\alpha}$; K_d=6.1 MN/m.

10-storey building

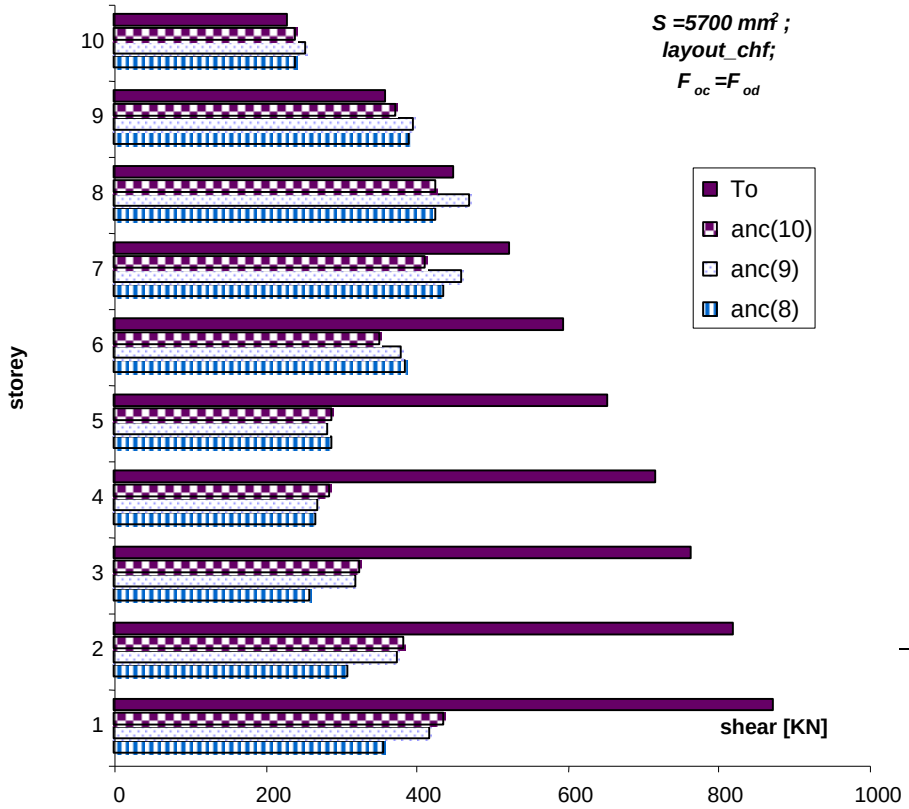

Fig. 3.5.3. Storey shears obtained for upper anchorage level at 10-th, 9-th or 8-th floors.
CHF layout; S_c=5700 mm^2; $F_{od}=F_{oc}=K_c\Delta l_{oc}/2$; C=100 kN(s/m)$^{\alpha}$; K_d=6.1 MN/m.

4-storey building

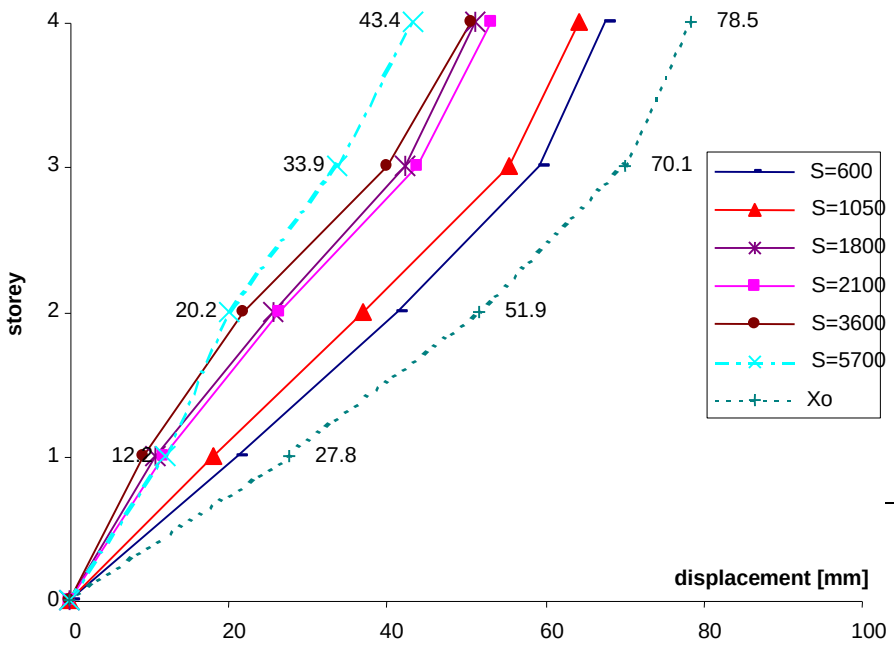

Fig. 3.6.1. Storey displacement as a function of S_c.

CHF layout; $F_{od}=F_{oc}=K_c\Delta l_{oc}/2$; $C=60$ kN(s/m)$^{\alpha}$; $K_d=6.1$ MN/m.

8-storey building

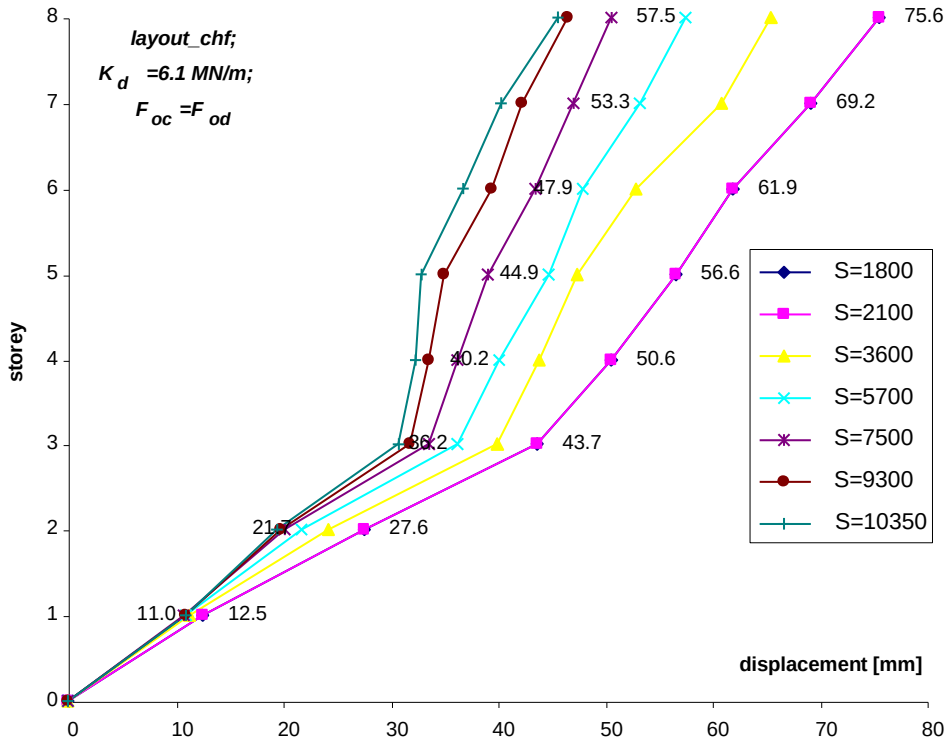

Fig. 3.6.2. Storey displacement as a function of S_c.

CHF layout; $F_{od}=F_{oc}=K_c\Delta l_{oc}/2$; $C=60$ kN(s/m)$^{\alpha}$; $K_d=6.1$ MN/m.

EC8 designed
4-storey building

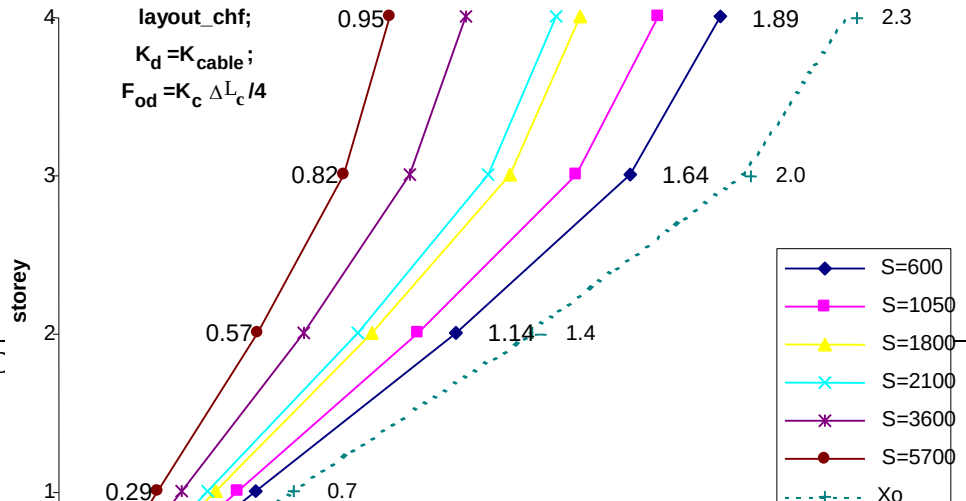

3.2.4.1

Fig. 3.6.3. Storey displacement as a function of S_c.

CHF layout; $F_{od}=F_{oc}=K_c\Delta l_{oc}/2$; $C=60$ kN(s/m)$^{\alpha}$; $K_d=6.1$ MN/m; $K_c=K_d$.

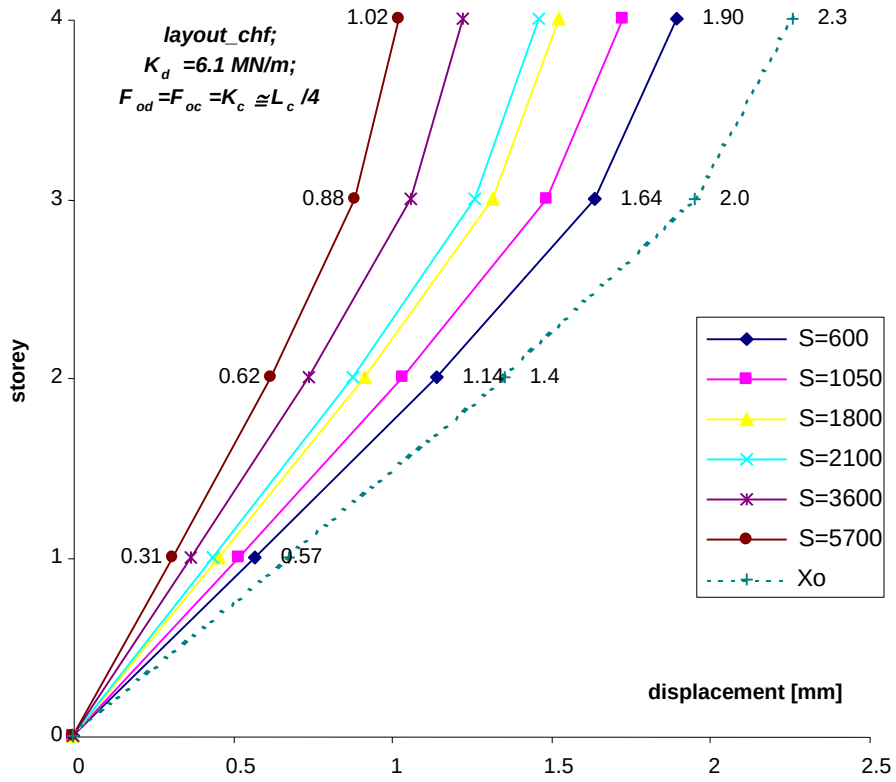

Fig. 3.6.4. Storey displacement as a function of S_c and K_c.

CHF layout; $F_{od}=F_{oc}=K_c\Delta l_{oc}/2$; $C=60$ kN(s/m)$^{\alpha}$; $K_d=6.1$ MN/m; $K_c=K_d$.

4 Conclusive remarks

As a general outcome of the investigation carried out, damped cable system showed a high potential as advanced seismic protection technology, and particularly for rather flexible structures, where damping effects can be entirely activated.
The following main suggestions emerged from the analysis in order to reach the best performance of this system:

- To select a F_{oc} level high enough to keep the cable in tension under the maximum considered design seismic action;
- To impose $F_{od}=F_{oc}$, so that the damper action can be suddenly activated when the cable pretension threshold is attained;
- To locate and select the C value minimising interstorey drift and storey shear response for each design case study (the minimum generally corresponds to the low-to-medium C values of the range of damping coefficients that characterizes on the whole the Jarret devices in ordinary production) .

Concerning cable layouts, the CHF and Pol2 configurations showed the best results, due to their capability to provide an optimal distribution of response quantities along the height, after proper calibration of the main mechanical parameters of the system.